Safe and Stable Connected Cruise Control for Connected Automated Vehicles With Response Lag

Yuchen Chen, *Graduate Student Member, IEEE*, Gábor Orosz, *Senior Member, IEEE*, and Tamas G. Molnar, *Member, IEEE*

***Abstract*—Controlling connected automated vehicles (CAVs) via vehicle-to-everything (V2X) connectivity holds significant promise for improving fuel economy and traffic efficiency. However, ensuring safety, especially in the presence of response lags, is critical for their real-world deployment. In this paper, we investigate the safety and stability of CAVs executing connected cruise control (CCC) by considering a first-order lag in their dynamics. Specifically, we derive conditions for plant stability and head-to-tail string stability and draw the corresponding stability charts. Moreover, using control barrier function (CBF) theory, we derive parameters for a CCC strategy that ensure safety and represent them as safety charts. We show that these provably safe parameter choices may restrict the benefits of V2X connectivity, such as enhancing string stability and energy efficiency. To ensure safety under lag while retaining CCC performance, we propose a safety-critical CCC by incorporating a lag-aware, CBF-based safety filter into a performant, but not necessarily safe CCC. This filter intervenes only when necessary, minimally modifying the CCC input to maintain safety. Simulation studies using real traffic data show that the proposed approach ensures safety under lag while preserving the benefits of V2X connectivity.**

***Index Terms*—Connected automated vehicle, connected cruise control, safety-critical control, stability analysis, first-order lag.**

I. Introduction

THE promise of automated vehicles (AVs) to improve safety, passenger comfort, energy efficiency, and traffic flow has driven a surge of research and development in recent years. As a result, longitudinal controller designs for AVs such as adaptive cruise control (ACC) have been studied intensively [1], [2] and deployed extensively. Vehicle-to-everything (V2X) connectivity, which enables connected automated vehicles (CAVs) to exchange information with other road users, can further enhance AV performance. With more information about the surrounding traffic, strategies like cooperative adaptive cruise control (CACC) [3] enable platoons of CAVs to drive cooperatively to save energy [4] and achieve string stability [5]. These benefits can be achieved, for example, using robust model predictive control (MPC) [6], [7], [8], [9] that overcomes real-world disturbances. Additionally, connected cruise control (CCC) [10], [11], which controls the motion of a single CAV using the information shared by the preceding connected (but not necessarily automated) vehicles, outperforms ACC in experiments [12] and also shows other significant benefits, such as reduced traffic congestion [13] and improved energy consumption [14]. Alternatively, leading cruise control (LCC) [15] and connected traffic control (CTC) [16], which leverage information from preceding and following connected vehicles, can also be used by CAVs to smooth the traffic flow.

Safety is the top priority when deploying AVs and CAVs. To ensure safety, various safety-critical control approaches have been developed, including reachability analysis [17], formal methods [18], reinforcement learning [19], and MPC [20], [21]. For platoons of AVs, externally positive state-feedback controllers have been designed via pole placement to guarantee both string stability and collision avoidance, even in the presence of response lag [22]. Furthermore, the safety of mixed traffic, i.e., platoons including both AVs and human-driven vehicles (HVs), has been studied using reinforcement learning [23] and string stability analysis [24], [25], [26].

Recently, control barrier functions (CBFs) [27] have gained popularity for safety-critical control. CBFs offer certain advantages over the aforementioned methods, such as compatibility with existing control frameworks and low computational demands, which facilitate their real-world deployment. In particular, CBFs enable the synthesis of computationally lightweight safety filters that intervene only when necessary to enforce safety constraints, while allowing the existing controller to operate unaltered when safe, thereby preserving its performance. Owing to these benefits, CBF-based methods have been applied to ACC [27], [28], obstacle avoidance [29], lane changing [30], merging scenarios [31], and safe traffic control [32], with experimental validations [33]. Notably, CBFs were used in [34] to establish safe CCC for CAVs, which was followed by a thorough analysis in [35]. A robust and safe CCC design was proposed in [36] with experimental validation on a heavy-duty truck, while safe CCC with input delay was addressed in [37]. However, these studies focused on scenarios where the AV or CAV responds solely to the vehicle immediately ahead, while the impact of connectivity to multiple vehicles ahead on safety is yet to be explored.

Received 30 August 2024; revised 28 July 2025 and 13 March 2026; accepted 5 August 2026. Date of publication 2 September 2026; date of current version 3 November 2026. The Associate Editor for this article was A. Hajbabaie. *(Corresponding author: Yuchen Chen.)*

Yuchen Chen is with the Department of Mechanical Engineering, University of Michigan, Ann Arbor, MI 48109 USA (e-mail: ethanch@umich.edu).

Gábor Orosz is with the Department of Mechanical Engineering and the Department of Civil and Environmental Engineering, University of Michigan, Ann Arbor, MI 48109 USA (e-mail: orosz@umich.edu).

Tamas G. Molnar is with the Department of Mechanical Engineering, Cleveland State University, Cleveland, OH 44115 USA (e-mail: t.g.molnar@csuohio.edu).

Digital Object Identifier 10.1109/TITS.2026.3727135

1558-0016 © 2026 IEEE. All rights reserved, including rights for text and data mining, and training of artificial intelligence and similar technologies. Personal use is permitted, but republication/redistribution requires IEEE permission.
See https://www.ieee.org/publications/rights/index.html for more information.

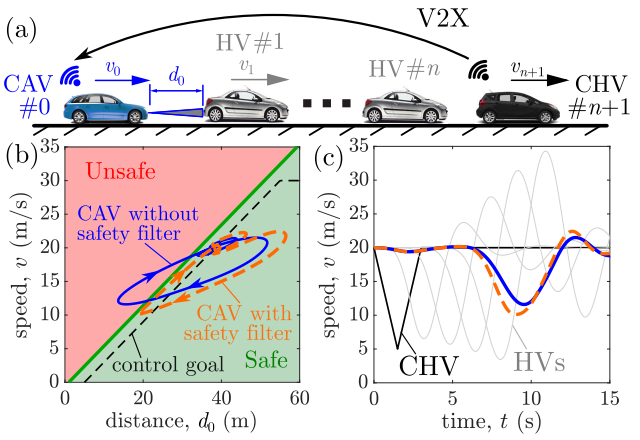


Fig. 1. (a) Using connected cruise control (CCC), a connected automated vehicle (CAV) responds to the preceding human-driven vehicle (HV) and to the lead connected human-driven vehicle (CHV) via vehicle-to-everything (V2X) connectivity. (b-c) Behavior of the CCC with unsafe control parameters (blue), and the proposed safety-critical CCC that modifies the above CCC to ensure safety with the help of a safety filter (orange).

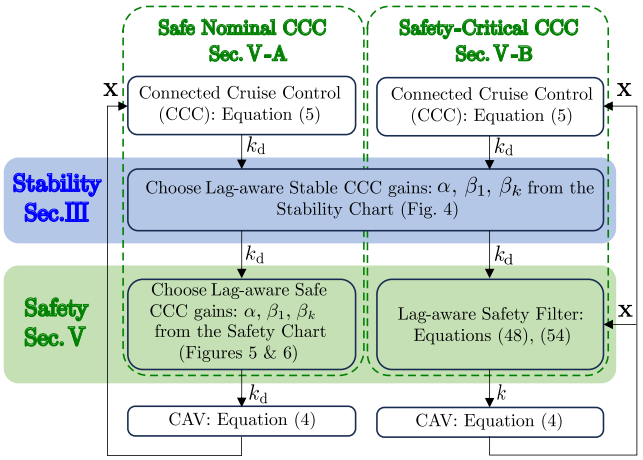


Fig. 2. Design process of the safe nominal CCC and safety-critical CCC.

Our recent work [38] investigated the safety of CCC in connected vehicle networks, where a CAV responds to a connected human-driven vehicle (CHV) farther ahead via V2X connectivity. There we assumed that the CAV is capable of executing acceleration commands immediately, and neglected the response time of CAVs that inevitably arise in practice. In this work, we extend our previous study [38] to investigate the safety of CAVs using CCC under actuator response lag. Unlike [22], which addresses safety for non-connected AV platoons, we focus on connected vehicle networks operating in mixed traffic environments, as illustrated in Fig. 1(a).

Specifically, this paper makes the following contributions:

- We establish a safe and stable CCC design which takes the CAV's response time into account as a first-order lag. We consider a general connectivity structure, where the CAV responds to multiple connected vehicles ahead, and potentially uses their acceleration information.
- We conduct plant and head-to-tail string stability analysis to identify the CCC parameter regions that ensure stable behavior under lag, and visualize them as stability charts.
- We derive sufficient conditions on the CCC parameter regions that guarantee safety and visualize them in safety charts. However, restricting the CCC to these safe gains may limit the performance benefits of connectivity.
- To ensure safety without sacrificing performance, we propose a safety-critical CCC that integrates a lag-aware safety filter. This allows the nominal CCC to operate normally when safe, preserving its benefits, and intervenes only when necessary to ensure safety; see Fig. 1(b–c).

Following the design process in Fig. 2, the rest of this paper is organized as follows. In Sec. II, we introduce the dynamics of HVs and the CAV, along with a nominal CCC algorithm. In Sec. III, we derive stability charts that identify CCC parameters ensuring plant and head-to-tail string stability. In Sec. IV, we review the background on CBFs, which will be used in the design of safe CCC. In Sec. V, we address safety using two approaches: (i) deriving sufficient safety conditions for the nominal CCC and visualizing them via safety charts (Sec. V-A); and (ii) proposing a safety-critical CCC by incorporating a lag-aware safety filter (Sec. V-B). We demonstrate the proposed approach through numerical simulations utilizing real traffic data. Finally, we conclude our results in Sec. VI.

II. Vehicle Dynamics and Connected Cruise Control

Consider a setup where a connected automated vehicle (CAV) is controlled to follow a chain of human-driven vehicles (HVs) on a single lane while responding to connected human-driven vehicles (CHVs) farther ahead. The CAV uses on-board sensors to evaluate its own speed v_0, the preceding HV's speed v_1, and the distance d_0 between them. Additionally, the CAV also receives the CHVs' speeds v_k through vehicle-to-everything (V2X) connectivity. An illustration of this setup is depicted in Fig. 1(a), where the CAV is only linked with one CHV that is $n+1$ vehicles ahead.

The dynamics of the HVs are represented by

$$\begin{aligned} \dot{d}_i(t) &= v_{i+1}(t) - v_i(t), \\ \dot{v}_i(t) &= u_i(t-\tau), \end{aligned} \tag{1}$$

for $i \in \{1,\dots,n\}$, where u_i is the HV's acceleration, and τ captures the driver reaction time and powertrain delays. We use the optimal velocity model (OVM) to characterize the human driver behavior during the car-following task [26], [39]:

$$u_i = \alpha_{\mathrm{h},i}\big(V_i(d_i) - v_i\big) + \beta_{\mathrm{h},i}\big(v_{i+1} - v_i\big), \tag{2}$$

for $i \in \{1,\dots,n\}$. In this model, each HV's acceleration is determined by the speed difference with gain $\beta_{\mathrm{h},i}$ and by the distance with gain $\alpha_{\mathrm{h},i}$ and the range policy

$$V_i(d) = \min\{\kappa_i(d - d_{\mathrm{st}}), v_{\max}\}, \tag{3}$$

for $i \in \{1,\dots,n\}$. This policy outlines a target velocity determined by the distance to the vehicle ahead, which is zero at the standstill distance d_{st} and grows linearly with gradient κ_i up to the speed limit $v_{\max}$.

Since a CAV typically exhibits a smaller response delay than a HV, for simplicity, we model the CAV's dynamics by approximating its response time as a first-order lag ξ, yielding

$$\begin{aligned}\dot{d}_0(t) &= v_1(t) - v_0(t),\\ \dot{v}_0(t) &= a_0(t),\\ \dot{a}_0(t) &= \frac{1}{\xi}\big(u_0(t) - a_0(t)\big).\end{aligned} \tag{4}$$

The CAV executes the acceleration command u_0, while its actual acceleration a_0 has lag ξ. Note that when $\xi \to 0$, $u_0(t) \equiv a_0(t)$ and system (4) can be simplified to the first two equations. For simplicity, we neglect the rolling and air resistances of the CAV, which could potentially reduce speed and improve safety. We also omit input constraints, since well-designed safety criteria and controllers can successfully prevent the input from reaching the physical limit, as demonstrated later. Notably, safety-critical control with input constraints remains an open problem. This is addressed in the context of control barrier functions, for example, in [40], [41], and [42].

For car-following purposes, we implement a desired controller $u_0 = k_{\rm d}(\mathbf{x})$ for the CAV, which responds to the state $\mathbf{x} = [\, d_0 \;\; v_0 \;\; a_0 \,]^\top$. Specifically, we select the connected cruise control (CCC) strategy, which was first presented in [10] and [11] and experimentally validated in [12]. Here we follow [11], but with slightly changed notation that fits our purposes:

$$\begin{aligned}k_{\rm d}(\mathbf{x}) = \alpha\big(V(d_0) - v_0\big) + \beta_1\big(W(v_1) - v_0\big)\\ + \sum_{k\in\Phi}\beta_k\big(W(v_k) - v_0\big).\end{aligned} \tag{5}$$

Here the CAV responds to the distance from and velocity of the vehicle ahead with gains α and β_1, respectively, and also to the speeds of CHVs with gains $\beta_k (k > 1)$. Also, v_k denotes the speed of the CHV k vehicles ahead, and Φ denotes the set of indices corresponding to the CHVs whose velocities are accessible to the CAV via connectivity. For instance, in Fig. 1(a), the CAV only connects to CHV #n+1, thus $\Phi = \{n+1\}$. In this case, (5) becomes

$$\begin{aligned}k_{\rm d}(\mathbf{x}) = \alpha\big(V(d_0) - v_0\big) + \beta_1\big(W(v_1) - v_0\big)\\ + \beta_{n+1}\big(W(v_{n+1}) - v_0\big).\end{aligned} \tag{6}$$

When the CAV only responds to the vehicle immediately ahead ($\Phi = \emptyset$), CCC (5) only contains distance and speed difference terms with gains α and β_1, resembling an adaptive cruise controller as in [1], where V2X connectivity is not required. CCC also executes the range policy

$$V(d) = \min\{\kappa(d - d_{\rm st}), v_{\max}\}, \tag{7}$$

which is similar to (3), and the speed policy

$$W(v) = \min\{v, v_{\max}\}, \tag{8}$$

to ensure it does not exceed the speed limit.

Note that CCC (5) does not always provide formal safety guarantees. In particular, a CCC design that is safe for a lag-free case may violate safety once actuator lag is introduced. This is illustrated in Fig. 3, where the CAV in (4) is simulated without lag ($\xi = 0$ s) and with lag ($\xi = 2$ s) using CCC (6)

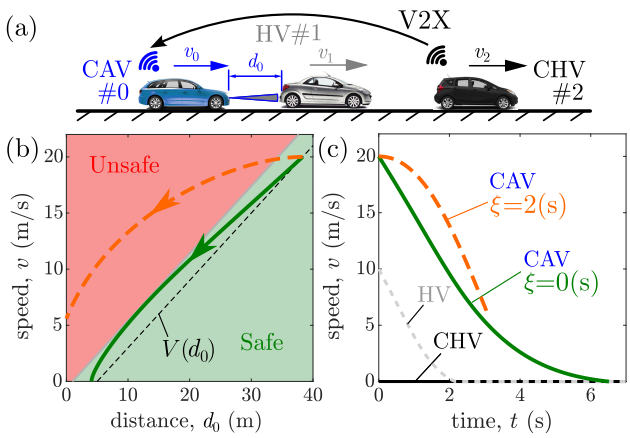


Fig. 3. A CCC law in (6) that ensures collision avoidance for the lag-free CAV (green) can lead to a collision for the CAV (4) with lag $\xi = 2$ s (orange).

with $\alpha = 0.6\ \text{s}^{-1}$, $\beta_1 = 0.3\ \text{s}^{-1}$ and $\beta_2 = 0.1\ \text{s}^{-1}$. Here, the CAV applies harsh braking to avoid a collision with the preceding HV while responding to a stopped CHV in front. As shown by Fig. 3(b-c), the lag-free CAV (green) brakes immediately and successfully avoids crashing. In contrast, applying the same CCC gains to a CAV with lag (orange) results in a collision. This example highlights the necessity of lag-aware CCC design to provide formal safety guarantees. Motivated by this observation, we next formally analyze how lag affects the safety of CAVs executing CCC (5). Moreover, we propose a novel lag-aware safety-critical CCC ensuring provable safety under lag while preserving nominal performance. Before the safety analysis, we first provide a guide for designing a stable CCC as preliminary.

III. Stable CCC Design

Realizing stable behaviors for the CAV and the vehicle chain is a fundamental requirement for CCC. In this section, we derive the CCC parameter domains that guarantee plant and head-to-tail string stability [10], [11], [26] for the vehicle chain containing one CAV at the tail, and multiple HVs or CHVs ahead, such as in Fig. 1(a). Plant stability indicates that a vehicle can approach a constant-speed equilibrium in an asymptotically stable manner. Head-to-tail string stability means that velocity fluctuation of the tail vehicle is attenuated compared to that of the head vehicle as it propagates along the vehicle chain, which is critical for mitigating traffic congestion. Plant and head-to-tail string stability can be evaluated by calculating the so-called head-to-tail transfer function [11], which is established in the Laplace domain for the corresponding linearized dynamics.

To derive the head-to-tail transfer function, first we linearize the systems (1), (2) and (4), (5) around the equilibrium

$$d_i(t) \equiv d_i^*, \quad v_i(t) \equiv v^*, \quad a_i(t) \equiv 0, \tag{9}$$

for $i \in \{0, \ldots, n\}$, where all vehicles drive at the equilibrium speed v^*, while maintaining equilibrium distance d_i^* given by $v^* = V(d_0^*) = V_i(d_i^*)$ for $i \in \{1, \ldots, n\}$. Note that $v^* < v_{\max}$ must hold for the existence of the equilibrium, cf. (3), (7).

Then we define perturbations around the equilibrium as

$$\tilde{d}_i = d_i - d_i^*, \quad \tilde{v}_i = v_i - v^*, \quad \tilde{a}_i = a_i, \tag{10}$$

for $i \in \{0, \dots, n\}$, and consider state vectors with these perturbations as $\tilde{\mathbf{x}}_0 = [\,\tilde{d}_0 \;\; \tilde{v}_0 \;\; \tilde{a}_0\,]^\top$ for the CAV and $\tilde{\mathbf{x}}_i = [\,\tilde{d}_i \;\; \tilde{v}_i\,]^\top$ for the HVs where $i \in \{1, \dots, n\}$. The speed fluctuations are

$$\begin{aligned} \tilde{v}_0 &= \mathbf{C}_0 \tilde{\mathbf{x}}_0, \quad \mathbf{C}_0 = \begin{bmatrix} 0 & 1 & 0 \end{bmatrix}, \\ \tilde{v}_i &= \mathbf{C}_i \tilde{\mathbf{x}}_i, \quad \mathbf{C}_i = \begin{bmatrix} 0 & 1 \end{bmatrix}. \end{aligned} \tag{11}$$

After substituting (10) into (1), (2) and (4), (5), we linearize the nonlinear functions $V(.)$ and $W(.)$ for $0 < v_i^* < v_{\max}$, and derive the linearized models

$$\begin{aligned} \dot{\tilde{\mathbf{x}}}_0(t) &= \mathbf{A}_0 \tilde{\mathbf{x}}_0(t) + \mathbf{B}_{0,1} \tilde{v}_1(t) + \sum_{k \in \Phi} \mathbf{B}_{0,k} \tilde{v}_k(t), \\ \dot{\tilde{\mathbf{x}}}_i(t) &= \mathbf{A}_i \tilde{\mathbf{x}}_i(t) + \mathbf{A}_{i\tau} \tilde{\mathbf{x}}_i(t-\tau) \\ &\quad + \mathbf{B}_i \tilde{v}_{i+1}(t) + \mathbf{B}_{i\tau} \tilde{v}_{i+1}(t-\tau), \;\; \forall i \in \{1, \dots, n\}, \end{aligned} \tag{12}$$

with coefficient matrices $\mathbf{A}_0, \mathbf{B}_{0,1}, \mathbf{B}_{0,k}, \mathbf{A}_i, \mathbf{A}_{i\tau}, \mathbf{B}_i, \mathbf{B}_{i\tau}$ defined by (55) in Appendix. By applying the Laplace transform with zero initial condition, (11), (12) leads to

$$\begin{aligned} \tilde{V}_0(s) &= T_{0,1}(s) \tilde{V}_1(s) + \sum_{k \in \Phi} T_{0,k}(s) \tilde{V}_k(s), \\ \tilde{V}_1(s) &= \prod_{i=1}^{n} T_{i,i+1}(s) \tilde{V}_{n+1}(s), \\ \tilde{V}_k(s) &= \prod_{i=k}^{n} T_{i,i+1}(s) \tilde{V}_{n+1}(s). \end{aligned} \tag{13}$$

Here $\tilde{V}_0(s)$, $\tilde{V}_1(s)$, $\tilde{V}_k(s)$ and $\tilde{V}_{n+1}(s)$ denote the Laplace transforms of the speed perturbation of the CAV $\tilde{v}_0$, the preceding vehicles $\tilde{v}_1$, $\tilde{v}_k$ and the head vehicle $\tilde{v}_{n+1}$, respectively, while the link transfer functions are defined as

$$\begin{aligned} T_{0,1}(s) &= \mathbf{C}_0 (s\mathbf{I} - \mathbf{A}_0)^{-1} \mathbf{B}_{0,1}, \\ T_{0,k}(s) &= \mathbf{C}_0 (s\mathbf{I} - \mathbf{A}_0)^{-1} \mathbf{B}_{0,k}, \\ T_{i,i+1}(s) &= \mathbf{C}_i (s\mathbf{I} - \mathbf{A}_i - \mathbf{A}_{i\tau} \mathrm{e}^{-s\tau})^{-1} (\mathbf{B}_i + \mathbf{B}_{i\tau} \mathrm{e}^{-s\tau}), \end{aligned} \tag{14}$$

for $i \in \{1, \dots, n\}$ and $k \in \Phi$; see [11]. These link transfer functions can be obtained through the substitution of the coefficient matrices into (55), and their detailed expressions are given by (56) in Appendix.

The overall response of the vehicle chain considering speed perturbations from the head vehicle $\tilde{V}_{n+1}(s)$ to the tail vehicle $\tilde{V}_0(s)$ can be described by

$$\tilde{V}_0(s) = G_{0,n+1}(s) \tilde{V}_{n+1}(s), \tag{15}$$

where the head-to-tail transfer function can be expressed as

$$G_{0,n+1}(s) = T_{0,1}(s) \left(\prod_{i=1}^{n} T_{i,i+1}(s) + \sum_{k \in \Phi} T_{0,k}(s) \prod_{i=k}^{n} T_{i,i+1}(s) \right). \tag{16}$$

Considering the case shown in Fig. 1(a), i.e., CCC (6) with $\Phi = \{n+1\}$, (16) simplifies to

$$G_{0,n+1}(s) = T_{0,1}(s) \prod_{i=1}^{n} T_{i,i+1}(s) + T_{0,n+1}(s). \tag{17}$$

Using the head-to-tail transfer function, we can analyze the plant and head-to-tail string stability of the vehicle chain [43]. Plant stability is associated with the characteristic equation

$$\mathrm{D}(G_{0,n+1}(s)) = 0, \tag{18}$$

where D(.) denotes the denominator. Plant stability is achieved when all characteristic roots have a negative real part, i.e., $\mathrm{Re}(s_m) < 0$, $\forall m \in \mathbb{N}$. If a real root $s = 0$ lies on the imaginary axis, the system reaches the plant stability boundary

$$\mathrm{D}(G_{0,n+1}(0)) = 0. \tag{19}$$

Alternatively, the stability boundary is also reached if a complex conjugate pair of roots $s = \pm \mathrm{j}\Omega$, with $\mathrm{j}^2 = -1$ and $\Omega > 0$, is located at the imaginary axis, yielding

$$\begin{aligned} \mathrm{Re}(\mathrm{D}(G_{0,n+1}(\mathrm{j}\Omega))) &= 0, \\ \mathrm{Im}(\mathrm{D}(G_{0,n+1}(\mathrm{j}\Omega))) &= 0, \end{aligned} \tag{20}$$

where Re(.) and Im(.) denote the real and imaginary parts.

Head-to-tail string stability, on the other hand, describes whether velocity fluctuations are mitigated along the vehicle chain. According to (15), a velocity perturbation with frequency $\omega > 0$ from the head vehicle will be amplified by the ratio $\left|G_{0,n+1}(\mathrm{j}\omega)\right|$ when reaching the tail vehicle. Therefore, head-to-tail string stability can be achieved if and only if

$$\left|G_{0,n+1}(\mathrm{j}\omega)\right| < 1, \;\; \forall \omega > 0; \tag{21}$$

cf. [11]. Equation (21) is equivalent to $P(\omega) > 0$ with

$$P(\omega) := \frac{1}{\omega^2} \left(\mathrm{D}(\left|G_{0,n+1}(\mathrm{j}\omega)\right|^2) - \mathrm{N}(\left|G_{0,n+1}(\mathrm{j}\omega)\right|^2) \right), \tag{22}$$

where D(.) and N(.) denote denominator and numerator. For $\omega \to 0$, the string stability boundaries can be obtained by

$$\lim_{\omega \to 0} P(\omega) = 0. \tag{23}$$

For $\omega > 0$, a set of string stability boundaries, parameterized by the wave number $K \in [0, 2\pi)$, is provided in [44] as

$$G_{0,n+1}(\mathrm{j}\omega) = \frac{n_{\mathrm{R}}(\omega) + \mathrm{j} n_{\mathrm{I}}(\omega)}{d_{\mathrm{R}}(\omega) + \mathrm{j} d_{\mathrm{I}}(\omega)} = e^{-\mathrm{j}K}, \tag{24}$$

where $n_{\mathrm{R}}(\omega)$ and $n_{\mathrm{I}}(\omega)$ are the real and imaginary parts of $\mathrm{N}\big(G_{0,n+1}(\mathrm{j}\omega)\big)$, while $d_{\mathrm{R}}(\omega)$ and $d_{\mathrm{I}}(\omega)$ are those of $\mathrm{D}\big(G_{0,n+1}(\mathrm{j}\omega)\big)$.

Overall, (19), (20) define the plant stability boundaries, while (23), (24) specify the head-to-tail string stability boundaries, as a function of the CCC parameters α, β_1, β_k. Appendix provides the detailed formulas for these boundaries. Stability charts can be constructed from these formulas to illustrate the regions of the CCC parameters that provide plant and head-to-tail string stability for a vehicle chain, thus aiding stable CCC design.

An example of the stability charts in the (α, β_1) and (β_1, β_2) planes is provided in Fig. 4 for the scenario where a CAV responds to the CHV two vehicles ahead, using the parameters in Table I. Note that we assume the HV is plant stable but not necessarily string stable. In Fig. 4(b-c), the head-to-tail string stable region (blue) is enclosed by the boundaries (23) (blue lines) and (24) (rainbow colored curves for various values of K). This region can be concisely depicted as the string stable

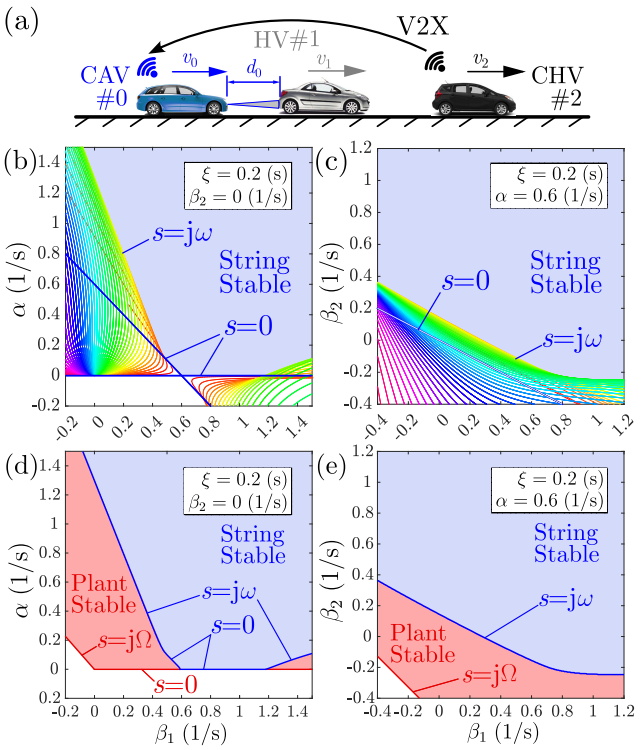


Fig. 4. Stability charts of a 3-vehicle chain including a CAV described by (4), (6) with $\xi = 0.2\,\mathrm{s}$ and $n = 1$, an HV given by (1), (2), and a CHV. (b-c) Head-to-tail string stable domains in the (α,β_1) plane and in the (β_1,β_2) plane. (d-e) Simplified string stable domains, along with plant stable regions.

TABLE I
PARAMETERS OF THE NUMERICAL CASE STUDIES

Vehicle	Variable	Symbol	Value	Unit
All	speed limit	$v_{\max}$	30	m/s
	standstill distance	d_{st}	5	m
	acceleration limit	$(a_{\min}, a_{\max})$	$(7, 3)$	m/s^2
HV	driver reaction delay	τ	0.9	s
	range policy gradient	κ_i	0.6	1/s
	driver gains	$(\alpha_{\mathrm{h},i}, \beta_{\mathrm{h},i})$	$(0.1, 0.6)$	1/s
CAV	performant gains (point Q)	$(\alpha, \beta_1, \beta_{n+1})$	$(0.6, 0.53, 0.5)$	1/s
	safe gains (point P)	$(\alpha, \beta_1, \beta_{n+1})$	$(0.6, 0.53, 0.03)$	1/s
	range policy gradient	κ	0.6	1/s
	safe distance	d_{sf}	1	m
	inverse time headway	κ_{sf}	0.6	1/s
	speed difference limit	$\bar{v}$	15	m/s
	CBF parameter	γ	1	1/s
	eCBF parameter	γ_{e}	1	1/s
CHV	speed perturbation	v_{pert}	15	m/s

domains in Fig. 4(d-e). The plant stable domains (red) are also plotted below the string stable domains, with boundaries determined by (19), (20). Note that the string stable region of the vehicle chain is inside the plant stable region.

IV. Background on Control Barrier Functions

In this section, we revisit the theory of control barrier functions, which is used to ensure the safety of the CCC (5).

Consider a control-affine system

$$\dot{\mathbf{x}} = \mathbf{f}(\mathbf{x}) + \mathbf{g}(\mathbf{x})\mathbf{u}, \tag{25}$$

where $\mathbf{x} \in \mathbb{R}^p$, $\mathbf{u} \in \mathbb{R}^q$ denote the state and the input, respectively, $\mathbf{f} : \mathbb{R}^p \to \mathbb{R}^p$ and $\mathbf{g} : \mathbb{R}^p \to \mathbb{R}^{p\times q}$ are locally Lipschitz continuous functions representing the dynamics. Given a locally Lipschitz continuous controller $\mathbf{k} : \mathbb{R}^p \to \mathbb{R}^q$, $\mathbf{u} = \mathbf{k}(\mathbf{x})$, we construct the closed-loop system

$$\dot{\mathbf{x}} = \mathbf{f}(\mathbf{x}) + \mathbf{g}(\mathbf{x})\mathbf{k}(\mathbf{x}), \tag{26}$$

which has the solution $\mathbf{x}(t)$ for the initial condition $\mathbf{x}(0) \in \mathbb{R}^p$. A *safe set* $\mathcal{S}$ is defined to determine the safety of system (26):

$$\mathcal{S} = \{\mathbf{x} \in \mathbb{R}^p : h(\mathbf{x}) \geq 0\}, \tag{27}$$

where $h : \mathbb{R}^p \to \mathbb{R}$ is a continuously differentiable function. With that, system (26) is considered safe w.r.t. $\mathcal{S}$ if

$$\mathbf{x}(0) \in \mathcal{S} \implies \mathbf{x}(t) \in \mathcal{S}, \quad \forall t \geq 0, \tag{28}$$

which means that if the system starts within the safe set, it should always remain there. Safety can be ensured by satisfying Nagumo's theorem [45] given below.

Theorem 1 ([45]): Let h satisfy $\nabla h(\mathbf{x}) \neq \mathbf{0}$ for all $\mathbf{x} \in \mathbb{R}^p$ such that $h(\mathbf{x}) = 0$. System (26) is safe w.r.t. $\mathcal{S}$ if and only if

$$\dot{h}\big(\mathbf{x}, \mathbf{k}(\mathbf{x})\big) \geq 0, \quad \forall \mathbf{x} \in \mathbb{R}^p \text{ s.t. } h(\mathbf{x}) = 0, \tag{29}$$

where

$$\dot{h}\big(\mathbf{x}, \mathbf{k}(\mathbf{x})\big) = \underbrace{\nabla h(\mathbf{x})\mathbf{f}(\mathbf{x})}_{L_{\mathbf{f}}h(\mathbf{x})} + \underbrace{\nabla h(\mathbf{x})\mathbf{g}(\mathbf{x})}_{L_{\mathbf{g}}h(\mathbf{x})}\mathbf{k}(\mathbf{x}), \tag{30}$$

and $L_{\mathbf{f}}h(\mathbf{x})$ and $L_{\mathbf{g}}h(\mathbf{x})$ denote the Lie derivatives.

Condition (29) is established at the boundary of $\mathcal{S}$, i.e., for $h(\mathbf{x}) = 0$, which prevents the system from leaving the safe set. However, it does not specify the system behavior within $\mathcal{S}$, i.e., for $h(\mathbf{x}) > 0$. To address this, control barrier functions (CBFs) [46] have been proposed to enable safety-critical controller synthesis for (25).

Definition 1 ([46]): Function h is a *control barrier function* for (25) on $\mathcal{S}$ if there exists $\Upsilon \in \mathcal{K}^{\mathrm{e}}$ such that for all $\mathbf{x} \in \mathcal{S}$

$$\sup_{\mathbf{u}\in\mathbb{R}^q} \dot{h}(\mathbf{x}, \mathbf{u}) > -\Upsilon\big(h(\mathbf{x})\big). \tag{31}$$

Remark 1: A continuous function $\Upsilon : \mathbb{R} \to \mathbb{R}$ is of extended class-$\mathcal{K}$ ($\Upsilon \in \mathcal{K}^{\mathrm{e}}$) if it is strictly increasing and $\Upsilon(0) = 0$. For example, the extended class-$\mathcal{K}$ function Υ is often chosen to be a linear function, $\Upsilon(r) = \gamma r$, with some $\gamma > 0$.

Theorem 2 ([46]): If h is a CBF for (25) on $\mathcal{S}$, then any locally Lipschitz continuous controller $\mathbf{k}$ that satisfies

$$\dot{h}\big(\mathbf{x}, \mathbf{k}(\mathbf{x})\big) \geq -\Upsilon\big(h(\mathbf{x})\big) \tag{32}$$

for all $\mathbf{x} \in \mathcal{S}$ renders (26) safe w.r.t. $\mathcal{S}$.

Note that when (32) is enforced outside $\mathcal{S}$, i.e., for all $\mathbf{x} \in \mathbb{R}^p \setminus \mathcal{S}$, it creates an attraction towards the safe set $\mathcal{S}$ [47].

CBFs are often used to design safety filters that minimally modify a desired but not necessarily safe controller $\mathbf{k}_{\mathrm{d}} : \mathbb{R}^p \to \mathbb{R}^q$ to a safe one, by solving the following quadratic programming problem with constraint (32) defined as

$$\begin{aligned} \mathbf{k}(\mathbf{x}) = \underset{\mathbf{u}\in\mathbb{R}^q}{\operatorname{argmin}} \ & \|\mathbf{u} - \mathbf{k}_{\mathrm{d}}(\mathbf{x})\|^2 \\ \text{s.t. } & \dot{h}(\mathbf{x}, \mathbf{u}) \geq -\Upsilon\big(h(\mathbf{x})\big). \end{aligned} \tag{33}$$

The closed-form solution of (33) was given in [36] as

$$\mathbf{k}(\mathbf{x}) = \begin{cases} \mathbf{k}_\mathrm{d}(\mathbf{x}) + \max\{0, \zeta(\mathbf{x})\} \dfrac{L_\mathbf{g}h(\mathbf{x})^\top}{\left\|L_\mathbf{g}h(\mathbf{x})\right\|^2}, & \text{if } L_\mathbf{g}h(\mathbf{x}) \neq \mathbf{0}, \\ \mathbf{k}_\mathrm{d}(\mathbf{x}), & \text{if } L_\mathbf{g}h(\mathbf{x}) = \mathbf{0}, \end{cases}$$
$$\zeta(\mathbf{x}) = -L_\mathbf{f}h(\mathbf{x}) - L_\mathbf{g}h(\mathbf{x})\mathbf{k}_\mathrm{d}(\mathbf{x}) - \Upsilon\big(h(\mathbf{x})\big). \tag{34}$$

For scalar input $u \in \mathbb{R}$ as in (4), the safety filter simplifies to

$$k(\mathbf{x}) = \begin{cases} \min\{k_\mathrm{d}(\mathbf{x}), k_\mathrm{s}(\mathbf{x})\}, & \text{if } L_\mathbf{g}h(\mathbf{x}) < 0, \\ k_\mathrm{d}(\mathbf{x}), & \text{if } L_\mathbf{g}h(\mathbf{x}) = 0, \\ \max\{k_\mathrm{d}(\mathbf{x}), k_\mathrm{s}(\mathbf{x})\}, & \text{if } L_\mathbf{g}h(\mathbf{x}) > 0, \end{cases} \tag{35}$$

with the safe controller

$$k_\mathrm{s}(\mathbf{x}) = -\frac{L_\mathbf{f}h(\mathbf{x}) + \Upsilon\big(h(\mathbf{x})\big)}{L_\mathbf{g}h(\mathbf{x})}. \tag{36}$$

By construction, the safety filter preserves the desired behavior from k_d when the system is safe, and seamlessly intervenes only when the CBF constraint (32) is activated to enforce safety. The closed-form solution enables efficient real-time implementation. Moreover, these formulations can be applied to nonlinear control-affine systems.

However, if $L_\mathbf{g}h(\mathbf{x}) \equiv \mathbf{0}$ for all $\mathbf{x} \in \mathcal{S}$, which occurs when a CBF designed for a lag-free CAV is directly applied to a lagged CAV, the safety of the system (26) cannot be affected by the controller $\mathbf{k}(\mathbf{x})$ from (30). Therefore, h cannot be used for synthesizing safety-critical controllers but an *extended CBF* $h_\mathrm{e} : \mathbb{R}^p \to \mathbb{R}$ [48], [49] can be constructed as

$$h_\mathrm{e}(\mathbf{x}) = L_\mathbf{f}h(\mathbf{x}) + \Upsilon\big(h(\mathbf{x})\big), \tag{37}$$

such that $L_\mathbf{g}h_\mathrm{e}(\mathbf{x}) \not\equiv \mathbf{0}$ with the *extended safe set*

$$\mathcal{S}_\mathrm{e} = \{\mathbf{x} \in \mathbb{R}^p : h_\mathrm{e}(\mathbf{x}) \geq 0\}. \tag{38}$$

Then, safety w.r.t. $\mathcal{S} \cap \mathcal{S}_\mathrm{e}$ can be established as follows.

Corollary 1 ([49]): If $L_\mathbf{g}h(\mathbf{x}) \equiv 0$ and h_e in (37) is a CBF for (25) on $\mathcal{S}_\mathrm{e}$ with $\Upsilon_\mathrm{e} \in \mathcal{K}^\mathrm{e}$, then any locally Lipschitz continuous controller $\mathbf{k}$ that satisfies

$$\dot{h}_\mathrm{e}\big(\mathbf{x}, \mathbf{k}(\mathbf{x})\big) \geq -\Upsilon_\mathrm{e}\big(h_\mathrm{e}(\mathbf{x})\big), \tag{39}$$

for all $\mathbf{x} \in \mathcal{S}_\mathrm{e}$ renders (26) safe w.r.t. $\mathcal{S} \cap \mathcal{S}_\mathrm{e}$.

Note that similar to Theorem 2, Υ_e can be chosen, for example, to be linear as $\Upsilon_\mathrm{e}(r) = \gamma_\mathrm{e} r$ with $\gamma_\mathrm{e} > 0$.

In this case, Nagumo's condition (Theorem 1) should be established at the boundary of $\mathcal{S} \cap \mathcal{S}_\mathrm{e}$, specifically when $h(\mathbf{x}) = 0$ and $h_\mathrm{e}(\mathbf{x}) \geq 0$, or when $h_\mathrm{e}(\mathbf{x}) = 0$ and $h(\mathbf{x}) \geq 0$. Here the former case implies $\dot{h}\big(\mathbf{x}, \mathbf{k}(\mathbf{x})\big) \geq 0$, which already satisfies (29), and thereby requires no further analysis. The Nagumo condition for the latter case is given as follows.

Corollary 2 ([35]): Let $L_\mathbf{g}h(\mathbf{x}) \equiv \mathbf{0}$ and h_e in (37) satisfy $\nabla h_\mathrm{e}(\mathbf{x}) \neq \mathbf{0}$ for all $\mathbf{x} \in \mathbb{R}^p$ such that $h_\mathrm{e}(\mathbf{x}) = 0$. System (26) is safe w.r.t. $\mathcal{S} \cap \mathcal{S}_\mathrm{e}$ if

$$\dot{h}_\mathrm{e}\big(\mathbf{x}, \mathbf{k}(\mathbf{x})\big) \geq 0, \quad \forall \mathbf{x} \in \mathbb{R}^p \text{ s.t. } h_\mathrm{e}(\mathbf{x}) = 0 \text{ and } h(\mathbf{x}) \geq 0. \tag{40}$$

For scalar input $u \in \mathbb{R}$ as in (4) and if $L_\mathbf{g}h_\mathrm{e}(\mathbf{x}) < 0$, (40) is equivalent to

$$k_\mathrm{s}(\mathbf{x}) \geq k(\mathbf{x}), \quad \forall \mathbf{x} \in \mathbb{R}^p \text{ s.t. } h_\mathrm{e}(\mathbf{x}) = 0 \text{ and } h(\mathbf{x}) \geq 0, \tag{41}$$

where the safe controller is

$$k_\mathrm{s}(\mathbf{x}) = -\frac{L_\mathbf{f}h_\mathrm{e}(\mathbf{x}) + \Upsilon_\mathrm{e}\big(h_\mathrm{e}(\mathbf{x})\big)}{L_\mathbf{g}h_\mathrm{e}(\mathbf{x})}, \tag{42}$$

cf. (36), and with h_e instead of h can be used in (35) to establish a safety filter according to Corollary 1.

V. Safe Connected Cruise Control

In this section, we first derive sufficient safety conditions for the nominal CCC (5) applied to the lagged CAV (4) via Corollary 2. These conditions provide CCC parameter regions that guarantee safety, thereby enabling safe nominal CCC design. Then we introduce a lag-aware safety-critical CCC that integrates a lag-aware safety filter via Corollary 1.

A. Safe Nominal CCC Design

Now we analyze the safety of the lagged CAV (4) executing the nominal CCC (5) based on condition (40), and propose a guideline for safe nominal CCC design.

First, we append the expression of the front vehicle's acceleration, i.e., $\dot{v}_1(t) = a_1(t)$, to the CAV dynamics (4), and write the system in the form of (25) with

$$\mathbf{x} = \begin{bmatrix} d_0 \\ v_0 \\ a_0 \\ v_1 \end{bmatrix}, \quad \mathbf{f}(\mathbf{x}) = \begin{bmatrix} v_1 - v_0 \\ a_0 \\ -\frac{a_0}{\xi} \\ a_1 \end{bmatrix}, \quad \mathbf{g}(\mathbf{x}) = \begin{bmatrix} 0 \\ 0 \\ \frac{1}{\xi} \\ 0 \end{bmatrix}. \tag{43}$$

Then, we select function h to characterize the CAV's safety. Several safety criteria were introduced in [35]. In this analysis, rather merely requiring a positive inter-vehicle distance, i.e., $d_0 > 0$, as in [22], we adopt a stricter criterion, which enforces larger distance at higher speeds. In particular, we mandate the *time headway* of the CAV $(d_0 - d_\mathrm{sf})/v_0$ to stay above the specified safe threshold $T_\mathrm{h} = 1/\kappa_\mathrm{sf}$, yielding

$$h(\mathbf{x}) = \kappa_\mathrm{sf}(d_0 - d_\mathrm{sf}) - v_0, \tag{44}$$

where d_sf is the safe standstill distance. The corresponding safe set $\mathcal{S}$ is defined in (27) and visualized as the green region in Fig. 1(b) and Fig. 3(b). The objective of the safe CCC is to keep the CAV within this region. By (43), (44), we have

$$\nabla h(\mathbf{x}) = \begin{bmatrix} \kappa_\mathrm{sf} & -1 & 0 & 0 \end{bmatrix} \neq \mathbf{0},$$
$$L_\mathbf{f}h(\mathbf{x}) = \kappa_\mathrm{sf}(v_1 - v_0) - a_0, \quad L_\mathbf{g}h(\mathbf{x}) \equiv 0. \tag{45}$$

Since $L_\mathbf{g}h(\mathbf{x}) \equiv 0$ for all $\mathbf{x} \in \mathcal{S}$, h in (44) is not a valid CBF. Thus, the extended CBF can be constructed as

$$h_\mathrm{e}(\mathbf{x}) = \kappa_\mathrm{sf}(v_1 - v_0) - a_0 + \gamma\big(\kappa_\mathrm{sf}(d_0 - d_\mathrm{sf}) - v_0\big), \tag{46}$$

where $\gamma > 0$ denotes the coefficient of the linear extended class-$\mathcal{K}$ function $\Upsilon(r) = \gamma r$; cf. (37). Then, we have

$$\nabla h_\mathrm{e}(\mathbf{x}) = \begin{bmatrix} \gamma\kappa_\mathrm{sf} & -\kappa_\mathrm{sf} - \gamma & -1 & \kappa_\mathrm{sf} \end{bmatrix} \neq \mathbf{0},$$
$$L_\mathbf{f}h_\mathrm{e}(\mathbf{x}) = \kappa_\mathrm{sf}(a_1 - a_0) + a_0/\xi + \gamma\big(\kappa_\mathrm{sf}(v_1 - v_0) - a_0\big),$$
$$L_\mathbf{g}h_\mathrm{e}(\mathbf{x}) = -1/\xi < 0. \tag{47}$$

Since Corollary 2 applies for h_e and the input u_0 is scalar, (41) can be used to determine whether a nominal CCC is safe.

Specifically, we choose the controller k in (41) as the nominal CCC (5), while safe controller k_s in (42) is given by

$$k_s(\mathbf{x}) = (1-\xi\kappa_{sf})a_0 + \xi\kappa_{sf}a_1 + \xi\gamma\big(\kappa_{sf}(v_1-v_0)-a_0\big) + \xi\gamma_e\Big(\kappa_{sf}(v_1-v_0)-a_0+\gamma\big(\kappa_{sf}(d_0-d_{sf})-v_0\big)\Big), \tag{48}$$

where $\gamma_e > 0$ denotes the coefficient of the linear extended class-$\mathcal{K}$ function $\Upsilon_e(r) = \gamma_e r$. By analyzing when condition (41) holds, safe choices of CCC gains α, β_1 and β_k, $\forall k \in \Phi$ can be derived as follows.

Theorem 3: The CAV (4) with $u_0 = k_d(\mathbf{x})$ given by CCC (5) and $\alpha \geq 0$, $\beta_1 \geq 0$, $\beta_k \geq 0$, $\forall k \in \Phi$ is safe w.r.t. $\mathcal{S} \cap \mathcal{S}_e$ given by (27), (38), (44), (46) if

- $v_0 \geq 0$, $|v_1 - v_0| \leq \bar{v}$, $|v_k - v_0| \leq \bar{v}$, $\forall k \in \Phi$ with some $\bar{v} > 0$;
- $a_1 \geq -a_{\min}$ with some $a_{\min} > 0$;
- $d_{st} > d_{sf}$, $\kappa_{sf} \geq \kappa > 0$, $\gamma > 0$;

and

$$\alpha \leq \frac{(1-\xi\kappa_{sf})^2}{4\xi} - \xi\left(\gamma - \frac{1-\xi\kappa_{sf}}{2\xi}\right)^2,$$
$$\alpha \geq \frac{\left(|\kappa_{sf} - \xi\kappa_{sf}^2 - \beta_1| + \sum_{k\in\Phi}\beta_k\right)\bar{v} + \xi\kappa_{sf}a_{\min}}{\kappa(d_{st}-d_{sf})}. \tag{49}$$

Please refer to Appendix for the proof.

Remark 2: Theorem 3 provides sufficient conditions for safety. Besides, the time headway criterion (44) is stricter than the collision avoidance requirement $d_0 > 0$. Therefore, CCC gains that violate (49) do not necessarily lead to a crash. In particular, for non-connected AV platoons, it has been shown in [22] that collision-free controller gains can be derived for arbitrarily large lag without input constraints.

Remark 3: The upper bound of α in (49) depends on γ, which can be chosen as $\gamma = (1-\xi\kappa_{sf})/(2\xi)$ to achieve the highest upper bound, i.e., largest region of safe control gains. In this case, $1/\xi > \kappa_{sf}$ should be satisfied to guarantee $\gamma > 0$. Unless specified otherwise, we consider $\gamma = (1-\xi\kappa_{sf})/(2\xi)$ and $1/\xi > \kappa_{sf}$ in the following calculations.

Remark 4: For unbounded velocity difference $\bar{v} \to \infty$, the safe region (49) becomes the single line segment given by

$$\frac{\xi\kappa_{sf}a_{\min}}{\kappa(d_{st}-d_{sf})} \leq \alpha \leq \frac{(1-\xi\kappa_{sf})^2}{4\xi},$$
$$\beta_1 = \kappa_{sf} - \xi\kappa_{sf}^2,\ \beta_k = 0,\ \forall k \in \Phi. \tag{50}$$

Theorem 3 characterizes a sufficient condition for nominal CCC that ensures safety under the time-headway criterion (44), which can be visualized as *safety charts*. For simplicity, we first visualize these charts for the two-vehicle case shown in Fig. 5(a), where the CAV only responds to the preceding CHV and the V2X connectivity is not required. The resulting charts are shown in Fig. 5(b–c), generated using the parameters in Table I for varying actuator lags ξ and speed difference bounds $\bar{v}$. The green regions indicate the safe choices of CCC parameters, from which a safe nominal CCC can be designed. In Fig. 5(b), as the lag increases, the upper horizontal boundary moves down and the lower V-shaped boundary moves towards smaller β_1 and larger α, shrinking the safe region. In Fig. 5(c), increasing the speed difference bound $\bar{v}$ causes the V-shaped

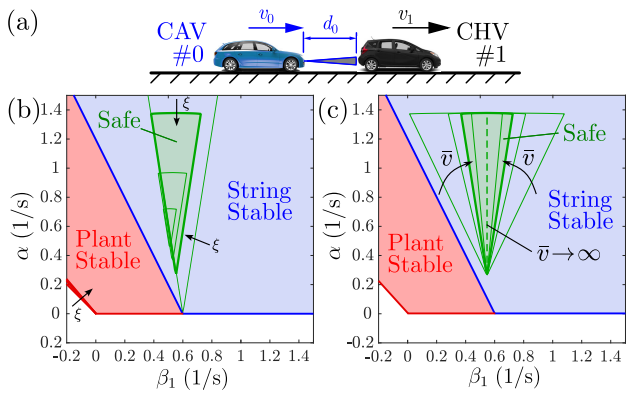


Fig. 5. Safety and stability charts of the CCC (5) with $\Phi = \emptyset$ where the CAV responds to the preceding CHV. Safety condition (49) is evaluated for (b) different CAV lags ($\xi = 0\,\text{s}, 0.15\,\text{s}, 0.2\,\text{s}, 0.25\,\text{s}$), and (c) various speed difference bounds ($\bar{v} = 5\,\text{m/s}, 10\,\text{m/s}, 15\,\text{m/s}, 25\,\text{m/s}$) with $\xi = 0.15\,\text{s}$.

safe region to narrow, gradually approaching the green dashed line given by (4). These trends indicate that the flexibility in selecting safe CCC gains decreases as the actuator lag and the speed difference bound increase. Nevertheless, for this scenario, it has been rigorously shown in [22] that collision-free controller gains can be derived for arbitrarily large lag.

Fig. 5(b-c) also visualizes the plant and head-to-tail string stability regions (red and blue), with boundaries defined by (59), (60), and (64), (67) for $\beta_{n+1} = 0$, respectively; see Appendix. Notably, except for extremely small $\bar{v}$, the safe domain consistently lies within the plant and string stable region, indicating that CCC safety requirements are aligned with stability requirements.

To illustrate the impact of V2X connectivity on safe nominal CCC design, we next examine the scenario where the CAV responds not only to the preceding HV but also to the CHV two vehicles ahead using CCC (6) with $n = 1$; see Fig. 6(a). Safety condition (49) is visualized in the (β_1, α) plane for various β_2 values, and in the (β_1, β_2) plane for various α values, using parameters from Table I and different lags ξ; see Fig. 6(b-g). As in Fig. 5(b), the safe regions (green) in Fig. 6(b), (d), (f) shrink as the lag increases. Indeed, the safe domains for $\beta_2 = 0$ match those presented in Fig. 5(b). Furthermore, the safe domain moves towards higher α values as β_2 increases, signifying that enhanced response to the head CHV's speed makes provable safe nominal CCC design more restrictive. This occurs because the CAV's safety requires prioritizing the response to the preceding HV, while increased response to the head CHV may disturb that response and lead to unsafe behavior. In Fig. 6(c),(e),(g), the safe region in the (β_1, β_2) plane shrinks to the "center" at $(\kappa_{sf} - \xi\kappa_{sf}^2, 0)$ as α decreases and as the lag increases. Since Theorem 3 provides only a sufficient condition, these safe regions may not provide all possible safe CCC gains, but they offer practical guidance for safe nominal CCC design.

The plant and head-to-tail string stable domains (red and blue) are also shown with boundaries specified in Appendix. As in Fig. 5, the safe domains in Fig. 6 remain within the stable region. However, head-to-tail string stability also depends on the HV's behavior. For a long vehicle chain with

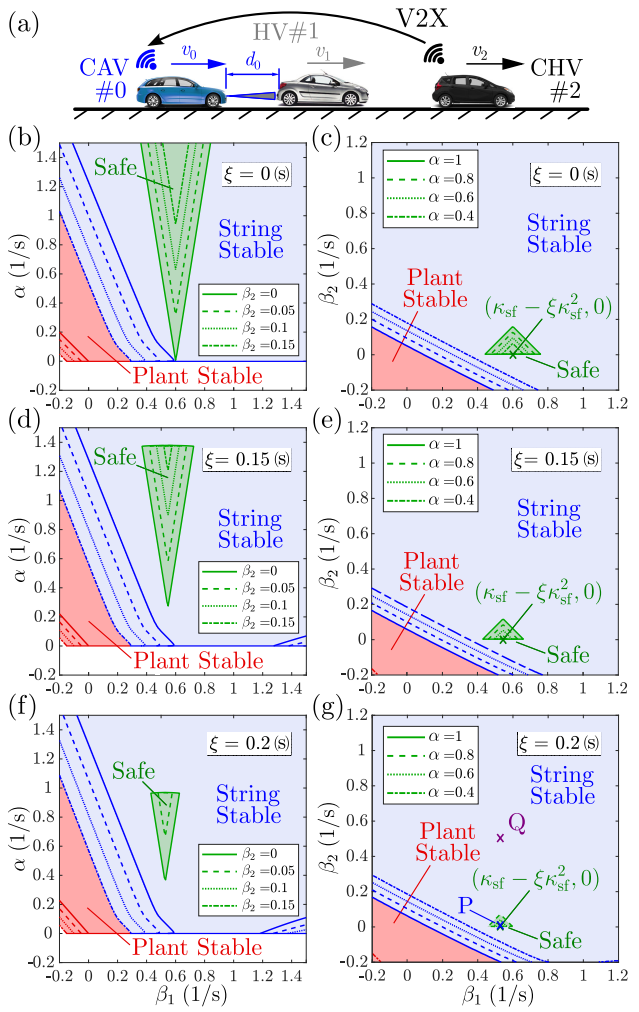


Fig. 6. Safety and stability charts of the CCC (6) with $n = 1$ where the CAV responds to the HV, and the CHV two vehicles ahead. Safety condition (49) is considered for the lag (b-c) $\xi = 0$ s; (d-e) $\xi = 0.15$ s; (f-g) $\xi = 0.2$ s.

string-unstable HVs, even safe CCC parameters may not guarantee head-to-tail string stability, while plant stability will still be ensured.

We remark that, in addition to CCC (5), a more general form of CCC could also be used, where the CAV not only responds to distance and speeds, but also to the HV's and CHV's accelerations [10]:

$$k_{\rm d}(\mathbf{x}) = \alpha\big(V(d_0) - v_0\big) + \beta_1\big(W(v_1) - v_0\big) + \sum_{k\in\Phi}\beta_k\big(W(v_k) - v_0\big) + \eta_1 a_1 + \sum_{k\in\Phi}\eta_k a_k. \tag{51}$$

where η_1 and η_k are acceleration feedback gains.

Similar to Theorem 3, we derive the sufficient safety condition for nominal CCC (51) by analyzing when (41) holds.

Theorem 4: The CAV (4) with $u_0 = k_{\rm d}(\mathbf{x})$ given by CCC (51) and $\alpha \geq 0$, $\beta_1 \geq 0$, $\beta_k \geq 0$, $\forall k \in \Phi$, is safe *w.r.t.* $\mathcal{S} \cap \mathcal{S}_{\rm e}$ given by (27), (38), (44), (46) if

- $v_0 \geq 0$, $|v_1 - v_0| \leq \bar{v}$, $|v_k - v_0| \leq \bar{v}$, $\forall k \in \Phi$ with some $\bar{v} > 0$;
- $a_1, a_k \in [-\bar{a}, \bar{a}]$, $\forall k \in \Phi$ with some $\bar{a} > 0$;
- $d_{\rm st} > d_{\rm sf}$, $\kappa_{\rm sf} \geq \kappa > 0$, $\gamma > 0$;

and:

$$\frac{N_1\bar{v} + N_2\bar{a}}{\kappa(d_{\rm st} - d_{\rm sf})} \leq \alpha \leq \frac{(1 - \xi\kappa_{\rm sf})^2}{4\xi} - \xi\left(\gamma - \frac{1 - \xi\kappa_{\rm sf}}{2\xi}\right)^2, \tag{52}$$

where

$$N_1 = |\kappa_{\rm sf} - \xi\kappa_{\rm sf}^2 - \beta_1| + \sum_{k\in\Phi}\beta_k,$$
$$N_2 = |\xi\kappa_{\rm sf} - \eta_1| + \sum_{k\in\Omega}|\eta_k|. \tag{53}$$

Please refer to Appendix for the proof.

Overall, although the safety charts do not characterize all possible safe controllers, they offer a practical and verifiable guideline for safe nominal CCC design by selecting CCC parameters that satisfy (49), as shown by the green regions in Fig. 5 and Fig. 6. For non-connected AV platoons, collision-free string-stable controllers can be constructed for arbitrary large lag [22], without requiring an additional safety filter. In contrast, for connected mixed traffic scenarios as in Fig. 6(a), enforcing safety solely through tuning the nominal CCC may restrict the ability to exploit V2X connectivity for improved energy efficiency [21] and head-to-tail string stability [38]. To provide formal safety guarantees without sacrificing the benefits of connectivity, we next propose a lag-aware safety-critical CCC that decouples performance design from safety enforcement through a lag-aware CBF-based safety filter.

B. Safety-Critical CCC

Now we derive a safety-critical CCC by integrating a lag-aware safety filter (35) into the nominal CCC (5). Using the time headway criterion (44) and its corresponding extended CBF (46), and noting that $L_{\mathbf{g}}h_{\rm e}(\mathbf{x}) < 0$ from (47), the safety filter (35) simplifies to

$$k(\mathbf{x}) = \min\{k_{\rm d}(\mathbf{x}), k_{\rm s}(\mathbf{x})\}, \tag{54}$$

where the desired controller $k_{\rm d}$ is given by (5), and the safe controller $k_{\rm s}$ is obtained from (48). The safety filter computes $k_{\rm s}$ considering the CAV's current state $\mathbf{x}$ and the lag in its dynamics, then uses it to filter out the unsafe commands from the nominal CCC with minimal intervention in real time.

To evaluate the proposed controller, we first simulate a 3-vehicle scenario where the CAV responds to the CHV two vehicles ahead ($n = 1$); see Fig. 6(a). This simulation incorporates the lag $\xi = 0.2$ s and tests various controllers:

- safe nominal CCC (6) with safe gains P in Fig. 6(g),
- nominal CCC (6) with performant gains Q in Fig. 6(g),
- safety-critical CCC, i.e., nominal CCC (6) with performant gains Q and the lag-aware safety filter (48), (54).

Note that both CCC gains P and Q ensure plant and head-to-tail string stability as in Fig. 6(g), while gains Q adopt the larger β_{n+1} value, enabling stronger response to farther vehicle for improved performance [21], [26], [38]. The results are shown in Fig. 7(a-d) by teal, blue and orange dashed curves, respectively, using parameters from Table I.

In Fig. 7, all vehicles start at $v_i(0) = 25$ m/s, while the CAV has an initial distance $d_0(0) = V^{-1}\big(v_0(0)\big) = 46.7$ m. The CHV follows a prescribed speed perturbation $v_{\rm pert}$, first braking with

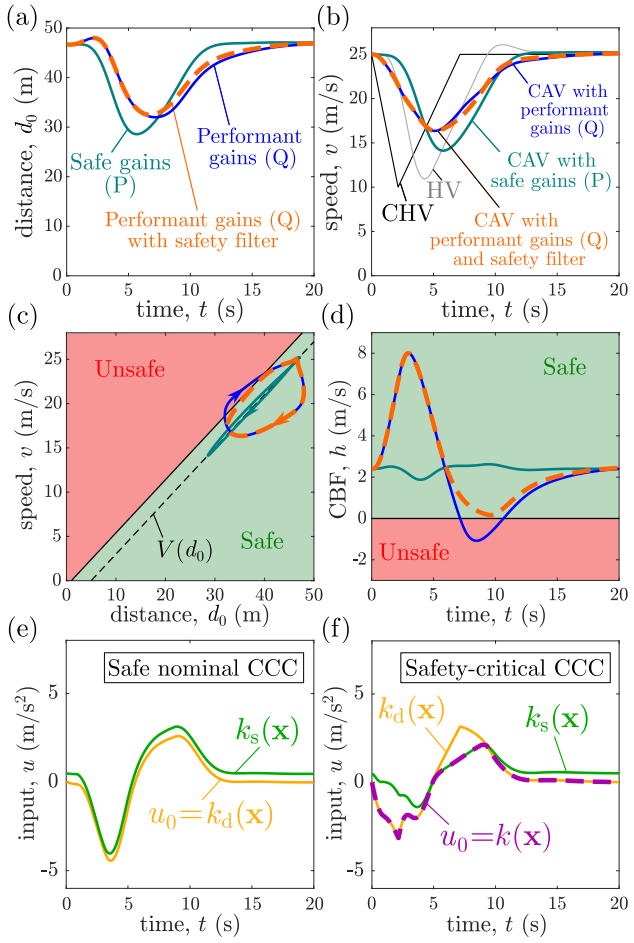


Fig. 7. (a-d) Simulations of CAV (4) for $\xi = 0.2$ s using CCC (6) with $n = 1$ for safe gains (teal) and performant gains (blue), and when using the safety-critical CCC (6), (48), (54) with a safety filter (orange). Desired inputs k_d and safe inputs k_s for (e) safe nominal CCC, and (f) safety-critical CCC, where u_0 indicates the controller input. The CHV follows a prescribed speed perturbation and the HV is simulated using (1), (2).

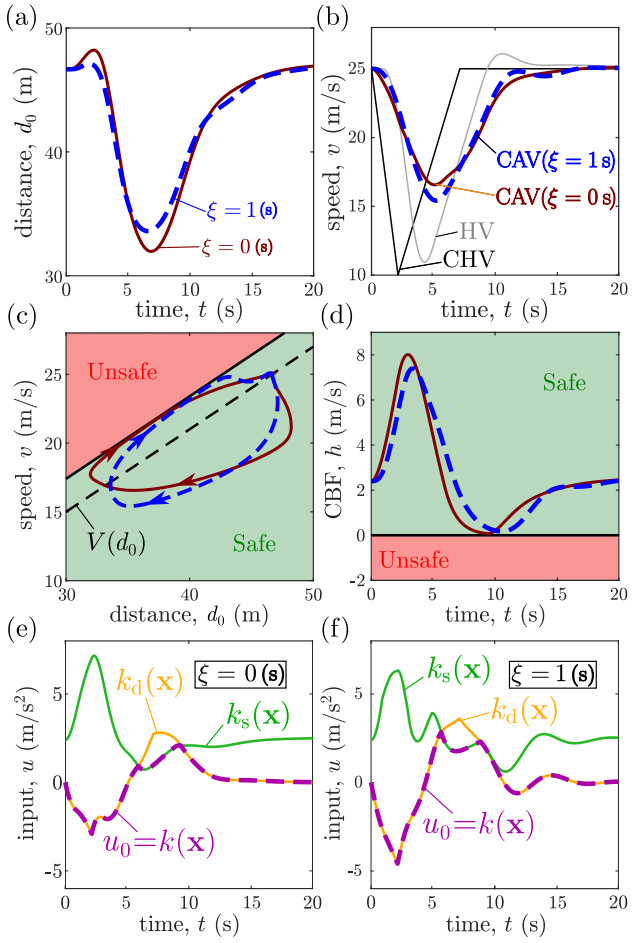


Fig. 8. (a-d) Simulations of CAV (4) for lags $\xi = 0$ s (dark red) and $\xi = 1$ s (dashed blue) using the safety-critical CCC (6), (48), (54) with $n = 1$ and performant gains Q. Desired inputs k_d, safe inputs k_s, and safety filter inputs k with (e) $\xi = 0$ s, and with (f) $\xi = 1$ s. The CHV follows a prescribed speed perturbation and the HV is simulated using (1), (2).

maximum deceleration $-a_{\min}$ and then recovering its initial speed using maximum acceleration $a_{\max}$. In all cases, the CAV is plant and head-to-tail string stable, as its speed fluctuation is smaller than that of the CHV; see Fig. 7(b). However, the CAV with performant gains (blue, orange) has smaller speed perturbations than with safe gains (teal), indicating improved string stability due to connectivity. In Fig. 7(c-d), the trajectory for safe gains P (teal) always stays inside the safe set, while the path for performant gains Q (blue) enters the unsafe region. However, the safety-critical CCC with performant gains Q (orange) successfully ensures safety by slightly altering the unsafe nominal CCC only when necessary.

This minimal safety filter intervention is further demonstrated by Fig. 7(e-f), which presents the nominal CCC input $k_d(\mathbf{x})$ from (6) and safe controller input $k_s(\mathbf{x})$ from (48). For safe nominal CCC in Fig. 7(e), $k_s(\mathbf{x})$ remains consistently higher than $k_d(\mathbf{x})$, indicating that the nominal CCC k_d can ensure safety and the safety filter does not need to be activated. In Fig. 7(f), the safety-critical CCC $k(\mathbf{x})$ remains the same as the nominal CCC $k_d(\mathbf{x})$ when safe, while the safety filter (54) intervenes when $k_d(\mathbf{x})$ exceeds $k_s(\mathbf{x})$ and alters the control input to $k_s(\mathbf{x})$ to ensure safety.

One may observe that the safety filter is activated during acceleration rather than deceleration; see the orange dashed curve in Fig. 7(b) and the purple dashed curve in Fig. 7(f). This occurs since the CAV matches its velocity to the head CHV. As the CHV decelerates, the CAV responds to it and brakes earlier than the HV, thereby increasing the distance and improving safety; see orange dashed curves in Fig. 7(a),(d). In this phase, the safety filter does not intervene, allowing the nominal CCC to enhance safety through connectivity. However, when the CHV accelerates after braking, the CAV also accelerates to match its velocity, even though the preceding HV still moves slower, resulting in rapidly decreasing distance; see Fig. 7(a-b). Although this could cause a safety violation for the nominal CCC (blue), the safety filter mitigates the acceleration and maintains a safe distance; see Fig. 7(f). Overall, the safety-critical CCC preserves the benefits of connectivity while also leveraging connectivity to improve safety.

To investigate the impact of the first-order lag ξ on the behavior of the safety-critical CCC (6), (48), (54), we simulate same scenario with same initial conditions as in Fig. 7. The resulting simulations in Fig. 8 incorporate lags $\xi = 0$ s and $\xi = 1$ s, using performant gains Q for the safety-critical CCC and the parameters in Table I.

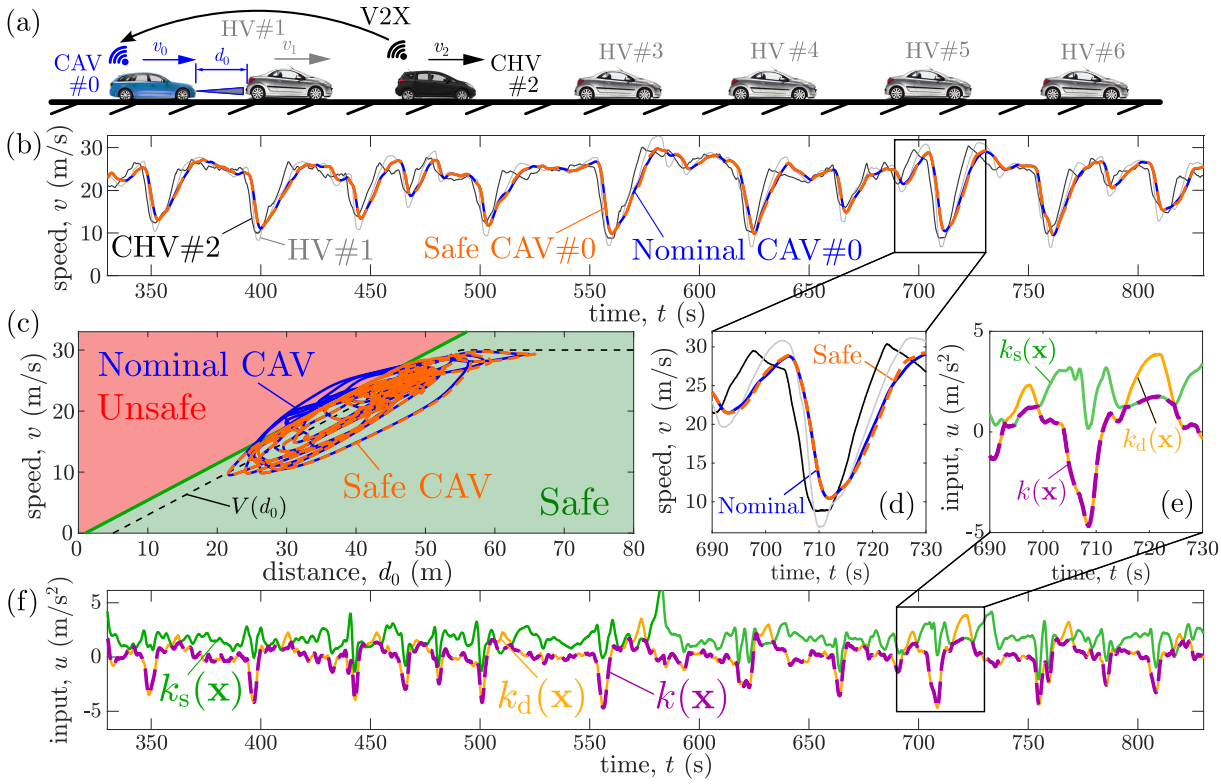


Fig. 9. Simulation of a vehicle chain where a CAV (4) responds to the CHV two vehicles ahead ($n = 1$, $\Phi = \{2\}$) with lag $\xi = 0.6$ s using the nominal CCC (5) (blue) and the safety-critical CCC (5), (48), (54) (orange). The speed profiles of the CHV and the HVs are real experiment data.

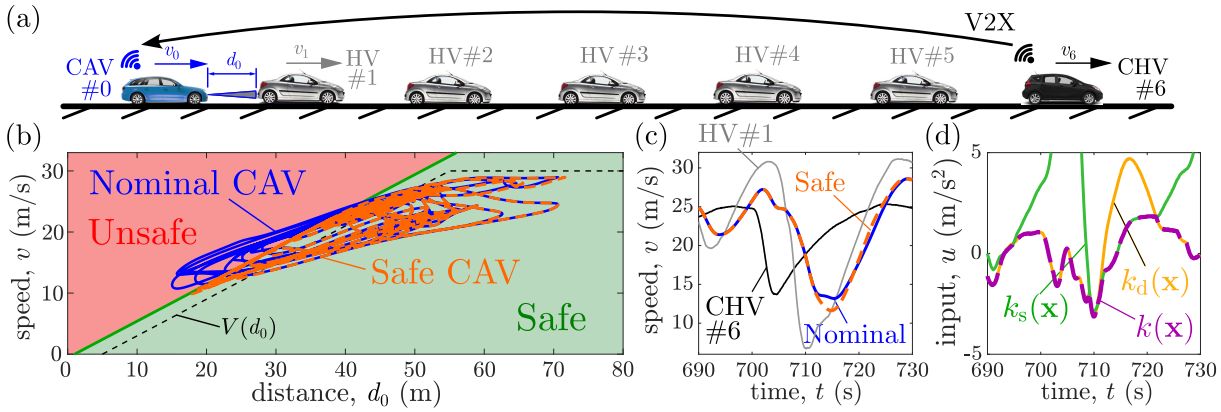


Fig. 10. Simulation of a vehicle chain where a CAV (4) responds to the CHV six vehicles ahead ($n = 5$, $\Phi = \{6\}$) with lag $\xi = 0.6$ s using the nominal CCC (5) (blue) and the safety-critical CCC (5), (48), (54) (orange). The speed profiles of the CHV and the HVs are real experiment data.

In Fig. 8(a-b), when the CHV decelerates, the CAV with a higher lag (blue) responds later and requires more pronounced braking to maintain a safe distance, which results in a larger speed perturbation. However, when the CHV accelerates, the higher-lag CAV responds later, while the HV simulatneously begins to accelerate. Thus, the lag enlarges the minimum distance, as shown in Fig. 8(a), thereby improving safety during acceleration and requiring less safety filter intervention. Importantly, the safety filter always provides safety guarantees regardless of lags, as the trajectories stay within the safe region in Fig. 8(c-d). Fig. 8(e-f) demonstrate safety filter intervention by comparing the nominal CCC $k_{\mathrm{d}}(\mathbf{x})$ in (6) and the safe controller $k_{\mathrm{s}}(\mathbf{x})$ in (48) for lags $\xi = 0$ s and $\xi = 1$ s. In both cases, the safety filter engages during CAV acceleration to mitigate the acceleration and keep safe distance (purple curves). For $\xi = 1$ s, it intervenes later and for a shorter period due to the CAV's later response to the CHV's acceleration.

To demonstrate that the proposed safety-critical CCC maintains safety and stability in real traffic, we explore the multi-vehicle scenarios shown in Fig. 9(a), Fig. 10(a), and Fig. 11(a), where the CAV is connected to the CHV two vehicles ahead ($n = 1$, $\Phi = \{2\}$), six vehicles ahead ($n = 5$, $\Phi = \{6\}$), and both of them ($\Phi = \{2, 6\}$), respectively. The speed profiles of the CHV and HVs, as well as the CAV's initial condition $\mathbf{x}(0) = [\,49.25 \;\; 22.94 \;\; 0\,]^{\top}$, are from real experimental data [12]. Fig. 9(b-d) and Fig. 10(b-c) present

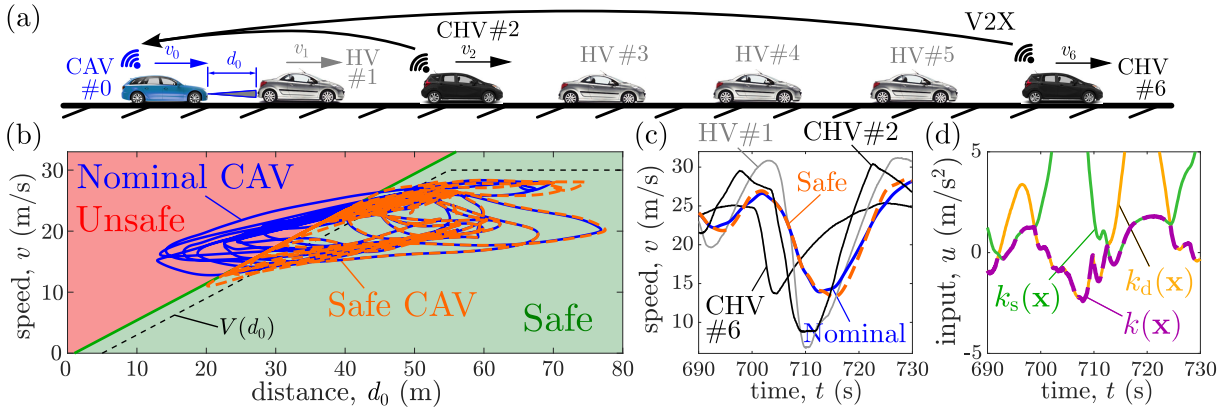


Fig. 11. Simulation of a vehicle chain where a CAV (4) responds to the CHVs two and six vehicles ahead ($\Phi = \{2, 6\}$, $\beta_2 = \beta_6 = 0.5$ s^{-1}) with lag $\xi = 0.6$ s using the nominal CCC (5) (blue) and the safety-critical CCC (5), (48), (54) (orange). The speed profiles of the CHVs and the HVs are real experiment data.

simulation results for CAVs with lag $\xi = 0.6$ s using nominal CCC (5) (blue) and safety-critical CCC (5), (48), (54) (orange), both with performant gains Q and parameters from Table I. Fig. 11(b-c) present results under the same setup, but with additional CCC gains $\beta_2 = \beta_6 = 0.5$ s^{-1}. Fig. 9(e-f), Fig. 10(d), and Fig. 11(d) show the safety filter's engagement by visualizing the nominal, safe, and safety-critical control inputs, denoted as $k_d(\mathbf{x})$, $k_s(\mathbf{x})$, and $k(\mathbf{x})$, respectively. Note that Fig. 10(c-d) and Fig. 11(c-d) correspond to Fig. 9(d-e).

Using V2X connectivity, all CAV controllers achieve considerably smaller speed perturbations than the preceding HV, as shown in Fig. 9(d), Fig. 10(c) and Fig. 10(c). However, only the safety-critical CCC successfully enforces safety constraint; see Fig. 9(c), Fig. 10(b), and Fig. 11(b). As above, the safety filter engages more frequently during CAV acceleration than deceleration; see Fig. 9(b),(f), Fig. 10(c-d), and Fig. 11(c-d). During deceleration, the CAV connected to farther and multiple CHVs ahead brakes earlier to synchronize with the CHV's speed, thus increasing the distance and enhancing safety; as indicated by the higher peak of $k_s(\mathbf{x})$ in Fig. 10(d) and Fig. 11(d) compared to Fig. 9(e). During acceleration, the CAV connected to farther and multiple CHVs ahead also accelerates earlier while the front HV is still traveling slowly; see the gray line in Fig. 10(c) and Fig. 11(c). This leads to a rapidly decreasing distance, necessitating safety filter intervention to mitigate acceleration and keep a safe distance.

The prolonged safety filter interventions are also evident from the longer duration when $k_d(\mathbf{x}) > k_s(\mathbf{x})$ in Fig. 10(d) and Fig. 11(d) compared to Fig. 9(e). Moreover, the behavior of $k_d(\mathbf{x})$ in Fig. 9(e), Fig. 10(d) and Fig. 11(d) shows that connecting to a farther CHV or multiple CHVs results in smoother deceleration and harsher acceleration. However, the safety filter significantly mitigates the acceleration, thereby reducing the control effort, lowering energy consumption, and enhancing comfort, as reflected in $k(\mathbf{x})$. That is, safety-critical CCC exploits V2X connectivity to enhance string stability while also guaranteeing safety at all times.

We remark that while the proposed safety-critical CCC assumes a fixed size for the vehicle chain, it retains a degree of robustness to vehicle cut-ins. A cut-in typically alters the CAV's state with a sudden reduction in distance to the front vehicle. If the state remains within the safe set after cutting in, safety is still guaranteed according to (28). If the state is pushed outside the safe set, provable safety guarantees no longer hold. However, the attraction created by the extended class-$\mathcal{K}$ function Υ in (32), (39) allows the proposed controller to drive the CAV back into the safe set if there is sufficient distance remaining for safe recovery.

VI. Conclusion

In this paper, we used control barrier function (CBF) theory to investigate the safety of connected automated vehicles (CAVs) implementing connected cruise control (CCC). In particular, we developed safety charts for existing CCC designs to provide safe control parameters. By comparing safety and stability charts, we showed that CAVs can achieve plant and head-to-tail string stability with safe CCC parameters. However, we found that these safe parameters may prevent fully exploiting V2X connectivity, especially under actuator lag, thereby limiting CCC performance. To overcome this limitation, we proposed the safety-critical CCC to guarantee provable safety under lag while preserving performance. We verified this controller via simulations using real traffic data, and highlighted that the proposed controller leverages connectivity to improve string stability, while the safety filter intervenes to prevent safety violations and reduce unnecessary control effort. In future research, we will compare the proposed controller with other safety-critical approaches, and expand it to multi-lane scenarios and nonlinear vehicle dynamics, including vehicle cut-ins and cut-outs.

Appendix

A. Expressions of Stability Boundaries

Here we provide the detailed calculations related to the stability analysis of Sec. III. We consider the case shown in Fig. 1, where a CAV follows the preceding HV while responding to the CHV that is $n + 1$ vehicles ahead using CCC (6). The resulting formulas (59), (60), (61) and (64), (65), (67), (68) were used in Fig. 4, Fig. 5 and Fig. 6 to

plot the plant stability (red) and head-to-tail string stability boundaries (blue), respectively.

Given the CAV's dynamics (4), (5) and HV's dynamics (1), (2), the coefficient matrices in (12) with $\Phi = \{n+1\}$ are

$$\mathbf{A}_0 = \begin{bmatrix} 0 & -1 & 0 \\ 0 & 0 & 1 \\ \frac{\alpha\kappa}{\xi} & -\frac{\Psi_0}{\xi} & -\frac{1}{\xi} \end{bmatrix}, \mathbf{B}_{0,1} = \begin{bmatrix} 1 \\ 0 \\ \frac{\beta_1}{\xi} \end{bmatrix}, \mathbf{B}_{0,n+1} = \begin{bmatrix} 0 \\ 0 \\ \frac{\beta_{n+1}}{\xi} \end{bmatrix},$$
$$\mathbf{A}_i = \begin{bmatrix} 0 & -1 \\ 0 & 0 \end{bmatrix}, \mathbf{A}_{i\tau} = \begin{bmatrix} 0 & 0 \\ \alpha_{\mathrm{h},i}\kappa_i & -\Psi_{\mathrm{h},i} \end{bmatrix},$$
$$\mathbf{B}_i = \begin{bmatrix} 1 \\ 0 \end{bmatrix}, \mathbf{B}_{i\tau} = \begin{bmatrix} 0 \\ \beta_{\mathrm{h},i} \end{bmatrix}, \tag{55}$$

with $\Psi_0 = \alpha + \beta_1 + \beta_{n+1}$, $\Psi_{\mathrm{h},i} = \alpha_{\mathrm{h},i} + \beta_{\mathrm{h},i}$ for $i \in \{1,\dots,n\}$. Substituting (55) into (14) leads to

$$T_{0,1}(s) = \frac{\beta_1 s + \alpha\kappa}{\xi s^3 + s^2 + \Psi_0 s + \alpha\kappa},$$
$$T_{0,n+1}(s) = \frac{\beta_{n+1} s}{\xi s^3 + s^2 + \Psi_0 s + \alpha\kappa},$$
$$T_{i,i+1}(s) = \frac{\beta_{\mathrm{h},i} s + \alpha_{\mathrm{h},i}\kappa_i}{e^{s\tau}s^2 + \Psi_{\mathrm{h},i} s + \alpha_{\mathrm{h},i}\kappa_i}, \ \forall i \in \{1,\dots,n\}. \tag{56}$$

Since $\mathrm{D}\big(T_{0,1}(s)\big) = \mathrm{D}\big(T_{0,n+1}(s)\big)$ given by (56), where D(.) denotes the denominator, from (17), the characteristic equation of the system is given by

$$\mathrm{D}\big(G_{0,n+1}(s)\big) = \mathrm{D}\big(T_{0,1}(s)\big) \times \prod_{i=1}^{n} \mathrm{D}\big(T_{i,i+1}(s)\big) = 0. \tag{57}$$

We assume that all HVs are plant stable, then $\mathrm{D}\big(T_{i,i+1}(s)\big) = 0 \implies \mathrm{Re}(s) < 0$ for $i \in \{1,\dots,n\}$, and the characteristic equation in (57) can be simplified to

$$\mathrm{D}(T_{0,1}(s)) = 0. \tag{58}$$

Equation (19) gives the plant stability boundary for $s = 0$. After substituting (56) and (58) into (19), we have

$$\alpha = 0. \tag{59}$$

The $s = \pm\mathrm{j}\Omega$ plant stability boundary is obtained by (20). By substituting $T_{0,1}(\mathrm{j}\Omega)$ from (56) and (58) into (20), we get the plant stability boundaries in the (α,β_1) space as

$$\alpha = \frac{\Omega^2}{\kappa}, \quad \beta_1 = \left(\xi - \frac{1}{\kappa}\right)\Omega^2 - \beta_{n+1}, \tag{60}$$

or the boundaries in the (β_1,β_{n+1}) space as

$$\beta_{n+1} = \alpha(\xi\kappa - 1) - \beta_1. \tag{61}$$

Equations (22) and (23) provide the $\omega = 0$ head-to-tail string stability boundary. After denoting the real and imaginary parts of the HVs' head-to-tail transfer function as $\Gamma_{\mathrm{R}}(\omega) = \mathrm{Re}\left(\prod_{i=1}^{n} T_{i,i+1}(\mathrm{j}\omega)\right)$, $\Gamma_{\mathrm{I}}(\omega) = \mathrm{Im}\left(\prod_{i=1}^{n} T_{i,i+1}(\mathrm{j}\omega)\right)$, while substituting (17) and (56) into (22), we have

$$P(\omega) = \alpha^2\kappa^2 \frac{1 - \Gamma_{\mathrm{I}}^2(\omega) - \Gamma_{\mathrm{R}}^2(\omega)}{\omega^2} - 2\alpha\kappa\left(\beta_{n+1}\frac{\Gamma_{\mathrm{I}}(\omega)}{\omega} + 1\right)$$
$$+ \alpha(\alpha + 2\beta_1 + 2\beta_{n+1}) + \mathcal{O}(\omega), \tag{62}$$

where $\mathcal{O}(\omega)$ denotes the higher order terms w.r.t. ω that vanish as $\omega \to 0$; cf. [43]. Note that $\mathcal{O}(\omega)$ contains the terms of $1 - \Gamma_{\mathrm{R}}(\omega)$ and $\Gamma_{\mathrm{I}}(\omega)$ since $\lim_{\omega\to 0}\Gamma_{\mathrm{R}}(\omega) = 1$ and $\lim_{\omega\to 0}\Gamma_{\mathrm{I}}(\omega) = 0$ hold. Then, one can get the $\omega = 0$ head-to-tail string stability boundary via (23) by taking the limit $\omega \to 0$. According to L'Hôpital's rule, we have

$$\lim_{\omega\to 0}\frac{\Gamma_{\mathrm{I}}(\omega)}{\omega} = -\sum_{i=1}^{n}\frac{1}{\kappa_i},$$
$$\lim_{\omega\to 0}\frac{1 - \Gamma_{\mathrm{I}}^2(\omega) - \Gamma_{\mathrm{R}}^2(\omega)}{\omega^2} = \sum_{i=1}^{n}\left(\frac{\alpha_{\mathrm{h},i} + 2\beta_{\mathrm{h},i} - 2\kappa_i}{\alpha_{\mathrm{h},i}\kappa_i^2}\right) = L_{\mathrm{h}}; \tag{63}$$

cf. [44]. By substituting (62) and (63) into (23), we can derive the $\omega = 0$ string stability boundary

$$\alpha = 0, \quad \alpha = -\frac{2\left(\beta_1 + \left(\sum_{i=1}^{n}\frac{\kappa}{\kappa_i} + 1\right)\beta_{n+1} - \kappa\right)}{L_{\mathrm{h}}\kappa^2 + 1}, \tag{64}$$

in the (α,β_1) space, and

$$\beta_1 = -\frac{(L_{\mathrm{h}}\kappa^2 + 1)}{2}\alpha - \left(\sum_{i=1}^{n}\frac{\kappa}{\kappa_i} + 1\right)\beta_{n+1} + \kappa, \tag{65}$$

in the (β_1,β_{n+1}) space.

Equation (24) defines the $\omega > 0$ head-to-tail string stability boundary, which can be rearranged into

$$d_{\mathrm{R}}(\omega) - n_{\mathrm{R}}(\omega)\cos K + n_{\mathrm{I}}(\omega)\sin K = 0,$$
$$d_{\mathrm{I}}(\omega) - n_{\mathrm{R}}(\omega)\sin K - n_{\mathrm{I}}(\omega)\cos K = 0. \tag{66}$$

Substituting (17) and (56) into (24) and solving it for α, β_1 and β_{n+1}, (66) yields the $\omega > 0$ head-to-tail string stability boundaries

$$\alpha = \frac{q_2 r_1 - q_1 r_2}{p_1 q_2 - p_2 q_1}, \quad \beta_1 = \frac{p_1 r_2 - p_2 r_1}{p_1 q_2 - p_2 q_1}, \tag{67}$$

in the (α,β_1) space, and

$$\beta_1 = \frac{q_4 r_3 - q_3 r_4}{p_3 q_4 - p_4 q_3}, \quad \beta_{n+1} = \frac{p_3 r_4 - p_4 r_3}{p_3 q_4 - p_4 q_3}. \tag{68}$$

in the (β_1,β_{n+1}) space, with coefficients

$$p_1 = \kappa(\Gamma_{\mathrm{R}}(\omega)\cos K - \Gamma_{\mathrm{I}}(\omega)\sin K - 1),$$
$$q_1 = p_3 = -\omega(\Gamma_{\mathrm{R}}(\omega)\sin K + \Gamma_{\mathrm{I}}(\omega)\cos K),$$
$$p_2 = p_4 = \kappa(\Gamma_{\mathrm{R}}(\omega)\sin K + \Gamma_{\mathrm{I}}(\omega)\cos K) - \omega,$$
$$q_2 = \omega(\Gamma_{\mathrm{R}}(\omega)\cos K - \Gamma_{\mathrm{I}}(\omega)\sin K) - \omega,$$
$$r_1 = \omega(\beta_{n+1}\sin K - \omega),$$
$$r_2 = \beta_{n+1}\omega(1 - \cos K) - \omega^3\xi,$$
$$q_3 = -\omega\sin K, \qquad q_4 = \omega(\cos K - 1),$$
$$r_3 = -p_1\alpha - \omega^2, \qquad r_4 = -p_2\alpha - \omega^3\xi. \tag{69}$$

B. Proof of Theorem 3

Proof: We prove safety via Corollary 2 by verifying that (41) holds. We express $k_{\mathrm{s}}(\mathbf{x}) - k_{\mathrm{d}}(\mathbf{x})$ by substituting (48) and (5):

$$k_{\mathrm{s}}(\mathbf{x}) - k_{\mathrm{d}}(\mathbf{x}) = \xi\gamma\big(\kappa_{\mathrm{sf}}(v_1 - v_0) - a_0\big) + (1 - \xi\kappa_{\mathrm{sf}})a_0$$
$$+ \xi\kappa_{\mathrm{sf}}a_1 + \xi\gamma_{\mathrm{e}}\big(\kappa_{\mathrm{sf}}(v_1 - v_0) - a_0 + \gamma(\kappa_{\mathrm{sf}}(d_0 - d_{\mathrm{sf}}) - v_0)\big)$$
$$- \alpha\big(V(d_0) - v_0\big) - \beta_1\big(W(v_1) - v_0\big) - \sum_{k\in\Phi}\beta_k\big(W(v_k) - v_0\big). \tag{70}$$

From (7), (8), we have $V(d_0) \leq \kappa(d_0 - d_{\rm st})$, $W(v_1) \leq v_1$, $W(v_k) \leq v_k$. Furthermore, we consider $h_{\rm e}(\mathbf{x}) = 0, \alpha \geq 0, \beta_1 \geq 0$, $\beta_k \geq 0$, $\forall k \in \Phi$, which yields

$$\begin{aligned} k_{\rm s}(\mathbf{x}) - k_{\rm d}(\mathbf{x}) \geq\ & (\xi\gamma + \xi\kappa_{\rm sf} - 1)\big(\kappa_{\rm sf}(v_1 - v_0) - a_0\big) \\ & + \xi\kappa_{\rm sf} a_1 + \big(\kappa_{\rm sf}(1 - \xi\kappa_{\rm sf}) - \beta_1\big)(v_1 - v_0) \\ & - \alpha\big(\kappa(d_0 - d_{\rm st}) - v_0\big) - \sum_{k\in\Phi}\beta_k\big(v_k - v_0\big). \end{aligned} \tag{71}$$

We then substitute $\kappa_{\rm sf}(v_1 - v_0) - a_0$ from $h_{\rm e}(\mathbf{x}) = 0$, i.e., $\kappa_{\rm sf}(v_1 - v_0) - a_0 = -\gamma\big(\kappa_{\rm sf}(d_0 - d_{\rm sf}) - v_0\big)$, while we add and subtract $\alpha h(\mathbf{x})$ on the right-hand side, which leads to

$$\begin{aligned} k_{\rm s}(\mathbf{x}) - k_{\rm d}(\mathbf{x}) \geq\ & \alpha(\kappa_{\rm sf} - \kappa)(d_0 - d_{\rm sf}) + \alpha\kappa(d_{\rm st} - d_{\rm sf}) \\ & - (\xi\gamma^2 + \xi\kappa_{\rm sf}\gamma - \gamma + \alpha)\big(\kappa_{\rm sf}(d_0 - d_{\rm sf}) - v_0\big) + \xi\kappa_{\rm sf} a_1 \\ & + (\kappa_{\rm sf} - \xi\kappa_{\rm sf}^2 - \beta_1)(v_1 - v_0) - \sum_{k\in\Phi}\beta_k\big(v_k - v_0\big). \end{aligned} \tag{72}$$

Since $h(\mathbf{x}) = \kappa_{\rm sf}(d_0 - d_{\rm sf}) - v_0 \geq 0$ is considered in (41), the third term on the right-hand side is nonnegative if

$$\begin{aligned} & \xi\gamma^2 + \xi\kappa_{\rm sf}\gamma - \gamma + \alpha \\ & = \xi\left(\gamma - \frac{1 - \xi\kappa_{\rm sf}}{2\xi}\right)^2 + \alpha - \frac{(1 - \xi\kappa_{\rm sf})^2}{4\xi} \leq 0, \end{aligned} \tag{73}$$

which holds given the upper bound on α in (49). Once (73) holds, (72) simplifies to

$$\begin{aligned} k_{\rm s}(\mathbf{x}) - k_{\rm d}(\mathbf{x}) \geq\ & \alpha(\kappa_{\rm sf} - \kappa)(d_0 - d_{\rm sf}) + \alpha\kappa(d_{\rm st} - d_{\rm sf}) \\ & + \xi\kappa_{\rm sf} a_1 - |\kappa_{\rm sf} - \xi\kappa_{\rm sf}^2 - \beta_1||v_1 - v_0| - \sum_{k\in\Phi}\beta_k|v_k - v_0|, \end{aligned} \tag{74}$$

where $d_0 - d_{\rm sf} \geq 0$ since $h(\mathbf{x}) \geq 0$ and $v_0 \geq 0$. Finally, considering $|v_1 - v_0| \leq \bar{v}$, $|v_k - v_0| \leq \bar{v}$, $\forall k \in \Phi$, $a_1 \geq -a_{\min}$, $\kappa_{\rm sf} \geq \kappa$, (72) leads to

$$\begin{aligned} & k_{\rm s}(\mathbf{x}) - k_{\rm d}(\mathbf{x}) \geq \alpha\kappa(d_{\rm st} - d_{\rm sf}) \\ & - \left(\big|\kappa_{\rm sf} - \xi\kappa_{\rm sf}^2 - \beta_1\big| + \sum_{k\in\Phi}\beta_k\right)\bar{v} - \xi\kappa_{\rm sf} a_{\min} \geq 0. \end{aligned} \tag{75}$$

Considering the lower bound on α in (49) and $d_{\rm st} > d_{\rm sf}$, (75) implies that (41) holds. Therefore, Corollary 2 provides safety and completes the proof. □

C. Proof of Theorem 4

Proof: Similar to the proof of Theorem 3, we prove safety by showing that (41) holds, where

$$\begin{aligned} k_{\rm s}(\mathbf{x}) - k_{\rm d}(\mathbf{x}) =\ & \xi\gamma\big(\kappa_{\rm sf}(v_1 - v_0) - a_0\big) + (1 - \xi\kappa_{\rm sf})a_0 \\ & + \xi\gamma_{\rm e}\big(\kappa_{\rm sf}(v_1 - v_0) - a_0 + \gamma(\kappa_{\rm sf}(d_0 - d_{\rm sf}) - v_0)\big) \\ & + (\xi\kappa_{\rm sf} - \eta_1)a_1 - \alpha\big(V(d_0) - v_0\big) - \beta_1\big(W(v_1) - v_0\big) \\ & - \sum_{k\in\Phi}\beta_k\big(W(v_k) - v_0\big) - \sum_{k\in\Phi}\eta_k a_k. \end{aligned} \tag{76}$$

Following the steps in (71)-(74), the inequality

$$\begin{aligned} k_{\rm s}(\mathbf{x}) - k_{\rm d}(\mathbf{x}) \geq\ & \alpha(\kappa_{\rm sf} - \kappa)(d_0 - d_{\rm sf}) + \alpha\kappa(d_{\rm st} - d_{\rm sf}) \\ & + (\xi\kappa_{\rm sf} - \eta_1)a_1 - |\kappa_{\rm sf} - \xi\kappa_{\rm sf}^2 - \beta_1||v_1 - v_0| \\ & - \sum_{k\in\Phi}\beta_k|v_k - v_0| - \sum_{k\in\Phi}\eta_k a_k, \end{aligned} \tag{77}$$

can be derived, where the additional acceleration feedback terms show up compared to (74). Considering $a_1, a_k \in [-\bar{a}, \bar{a}], \forall k \in \Phi$, we obtain

$$\begin{aligned} & k_{\rm s}(\mathbf{x}) - k_{\rm d}(\mathbf{x}) \geq \alpha\kappa(d_{\rm st} - d_{\rm sf}) \\ & - \left(\big|\kappa_{\rm sf} - \xi\kappa_{\rm sf}^2 - \beta_1\big| + \sum_{k\in\Phi}\beta_k\right)\bar{v} - \left(|\xi\kappa_{\rm sf} - \eta_1| + \sum_{k\in\Phi}|\eta_k|\right)\bar{a}, \end{aligned} \tag{78}$$

cf. (74). Using the lower bound on α in (52) and $d_{\rm st} > d_{\rm sf}$, we prove that (41) holds and Corollary 2 implies safety. □

REFERENCES

[1] G. Gunter et al., "Are commercially implemented adaptive cruise control systems string stable?" *IEEE Trans. Intell. Transp. Syst.*, vol. 22, no. 11, pp. 6992–7003, Nov. 2021.

[2] N. Bekiaris-Liberis, C. Roncoli, and M. Papageorgiou, "Predictor-based adaptive cruise control design," *IEEE Trans. Intell. Transp. Syst.*, vol. 19, no. 10, pp. 3181–3195, Oct. 2018.

[3] Z. Wang, G. Wu, and M. J. Barth, "A review on cooperative adaptive cruise control (CACC) systems: Architectures, controls, and applications," in *Proc. 21st IEEE Int. Conf. Intell. Transp. Syst.*, Nov. 2018, pp. 2884–2891.

[4] V. Turri, B. Besselink, and K. H. Johansson, "Cooperative look-ahead control for fuel-efficient and safe heavy-duty vehicle platooning," *IEEE Trans. Control Syst. Technol.*, vol. 25, no. 1, pp. 12–28, Jan. 2017.

[5] E. van Nunen, J. Reinders, E. Semsar-Kazerooni, and N. van de Wouw, "String stable model predictive cooperative adaptive cruise control for heterogeneous platoons," *IEEE Trans. Intell. Vehicles*, vol. 4, no. 2, pp. 186–196, Jun. 2019.

[6] P. Zhang et al., "Efficient robust model predictive control for behaviorally stable vehicle platoons," *IEEE Trans. Intell. Transp. Syst.*, vol. 26, no. 2, pp. 1671–1688, Feb. 2025.

[7] P. Zhang et al., "Joint optimization of platoon control and resource scheduling in cooperative vehicle-infrastructure system," *IEEE Trans. Intell. Vehicles*, vol. 8, no. 6, pp. 3629–3646, Jun. 2023.

[8] P. Zhang, D. Tian, J. Zhou, X. Duan, D. Zhao, and D. Cao, "A distributionally robust optimization model for vehicle platooning under stochastic disturbances," *IEEE Trans. Veh. Technol.*, vol. 73, no. 7, pp. 9666–9681, Jul. 2024.

[9] P. Zhang et al., "Efficient robust control of mixed platoon for improving fuel economy and ride comfort," *IEEE Trans. Veh. Technol.*, vol. 73, no. 9, pp. 12542–12555, Sep. 2024.

[10] J. I. Ge and G. Orosz, "Dynamics of connected vehicle systems with delayed acceleration feedback," *Transp. Res. C, Emerg. Technol.*, vol. 46, pp. 46–64, Sep. 2014.

[11] L. Zhang and G. Orosz, "Motif-based design for connected vehicle systems in presence of heterogeneous connectivity structures and time delays," *IEEE Trans. Intell. Transp. Syst.*, vol. 17, no. 6, pp. 1638–1651, Jun. 2016.

[12] J. I. Ge, S. S. Avedisov, C. R. He, W. B. Qin, M. Sadeghpour, and G. Orosz, "Experimental validation of connected automated vehicle design among human-driven vehicles," *Transp. Res. C, Emerg. Technol.*, vol. 91, pp. 335–352, Jun. 2018.

[13] Y. Qin, H. Wang, and B. Ran, "Control design for stable connected cruise control systems to enhance safety and traffic efficiency," *IET Intell. Transp. Syst.*, vol. 12, no. 8, pp. 921–930, Oct. 2018.

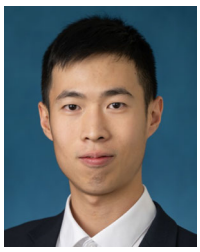
[14] M. Shen, C. R. He, T. G. Molnar, A. H. Bell, and G. Orosz, "Energy-efficient connected cruise control with lean penetration of connected vehicles," *IEEE Trans. Intell. Transp. Syst.*, vol. 24, no. 4, pp. 4320–4332, Apr. 2023.

[15] J. Wang, Y. Zheng, C. Chen, Q. Xu, and K. Li, "Leading cruise control in mixed traffic flow: System modeling, controllability, and string stability," *IEEE Trans. Intell. Transp. Syst.*, vol. 23, no. 8, pp. 12861–12876, Aug. 2022.

[16] T. G. Molnar and G. Orosz, "Destroying phantom jams with connectivity and automation: Nonlinear dynamics and control of mixed traffic," *Transp. Sci.*, vol. 58, no. 6, pp. 1319–1334, Nov. 2024.

[17] A. Alam, A. Gattami, K. H. Johansson, and C. J. Tomlin, "Guaranteeing safety for heavy duty vehicle platooning: Safe set computations and experimental evaluations," *Control Eng. Pract.*, vol. 24, pp. 33–41, Mar. 2014.

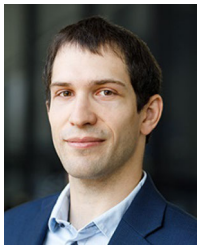
[18] P. Nilsson et al., "Correct-by-construction adaptive cruise control: Two approaches," *IEEE Trans. Control Syst. Technol.*, vol. 24, no. 4, pp. 1294–1307, Jul. 2016.
[19] L. Wen, J. Duan, S. E. Li, S. Xu, and H. Peng, "Safe reinforcement learning for autonomous vehicles through parallel constrained policy optimization," in *Proc. 23rd IEEE Int. Conf. Intell. Transp. Syst.*, Sep. 2020, pp. 1–7.
[20] C. Massera Filho, M. H. Terra, and D. F. Wolf, "Safe optimization of highway traffic with robust model predictive control-based cooperative adaptive cruise control," *IEEE Trans. Intell. Transp. Syst.*, vol. 18, no. 11, pp. 3193–3203, Nov. 2017.
[21] M. Shen, R. A. Dollar, T. G. Molnar, C. R. He, A. Vahidi, and G. Orosz, "Energy-efficient reactive and predictive connected cruise control," *IEEE Trans. Intell. Vehicles*, vol. 9, no. 1, pp. 944–957, Jan. 2024.
[22] A. Schwab and J. Lunze, "Design of platooning controllers that achieve collision avoidance by external positivity," *IEEE Trans. Intell. Transp. Syst.*, vol. 23, no. 9, pp. 14883–14892, Sep. 2022.
[23] Y. Cheng, C. Chen, X. Hu, K. Chen, Q. Tang, and Y. Song, "Enhancing mixed traffic flow safety via connected and autonomous vehicle trajectory planning with a reinforcement learning approach," *J. Adv. Transp.*, vol. 2021, pp. 1–11, Jun. 2021.
[24] W. B. Qin and G. Orosz, "Experimental validation of string stability for connected vehicles subject to information delay," *IEEE Trans. Control Syst. Technol.*, vol. 28, no. 4, pp. 1203–1217, Jul. 2020.
[25] D. Liu, B. Besselink, S. Baldi, W. Yu, and H. L. Trentelman, "On structural and safety properties of head-to-tail string stability in mixed platoons," *IEEE Trans. Intell. Transp. Syst.*, vol. 24, no. 6, pp. 6614–6626, Jun. 2023.
[26] G. Orosz and T. G. Molnár, *Dynamics and Control of Connected Vehicles*. Cham, Switzerland: Springer, 2025.
[27] A. Ames, J. Grizzle, and P. Tabuada, "Control barrier function based quadratic programs with application to adaptive cruise control," in *Proc. 53rd IEEE Conf. Decis. Control*, Dec. 2014, pp. 6271–6278.
[28] M. Waqas, M. Ali Murtaza, P. Nuzzo, and P. Ioannou, "Correct-by-construction design of adaptive cruise control with control barrier functions under safety and regulatory constraints," in *Proc. Amer. Control Conf. (ACC)*, Jun. 2022, pp. 5140–5146.
[29] Y. Chen, H. Peng, and J. Grizzle, "Obstacle avoidance for low-speed autonomous vehicles with barrier function," *IEEE Trans. Control Syst. Technol.*, vol. 26, no. 1, pp. 194–206, Jan. 2018.
[30] F. Hu and H. Yu, "Safety-critical lane-change control for CAV platoons in mixed autonomy traffic using control barrier functions," 2023, *arXiv:2302.00424*.
[31] V.-A. Le, H. M. Wang, G. Orosz, and A. A. Malikopoulos, "Coordination for connected automated vehicles at merging roadways in mixed traffic environment," in *Proc. 62nd IEEE Conf. Decis. Control (CDC)*, Dec. 2023, pp. 4150–4155.
[32] C. Zhao, H. Yu, and T. G. Molnar, "Safety-critical traffic control by connected automated vehicles," *Transp. Res. C*, vol. 154, p. 104230, Sep. 2023.
[33] G. Gunter, M. Nice, M. Bunting, J. Sprinkle, and D. B. Work, "Experimental testing of a control barrier function on an automated vehicle in live multi-lane traffic," in *Proc. Workshop Data-Driven Intell. Cyber-Phys. Syst. Smart Cities*, 2022, pp. 31–35.
[34] C. R. He and G. Orosz, "Safety guaranteed connected cruise control," in *Proc. 21st Int. Conf. Intell. Transp. Syst. (ITSC)*, Nov. 2018, pp. 549–554.
[35] T. G. Molnar, G. Orosz, and A. D. Ames, "On the safety of connected cruise control: Analysis and synthesis with control barrier functions," in *Proc. 62nd IEEE Conf. Decis. Control (CDC)*, Dec. 2023, pp. 1106–1111.
[36] A. Alan, A. J. Taylor, C. R. He, A. D. Ames, and G. Orosz, "Control barrier functions and input-to-state safety with application to automated vehicles," *IEEE Trans. Control Syst. Technol.*, vol. 31, no. 6, pp. 2744–2759, Nov. 2023.
[37] T. G. Molnar, A. K. Kiss, A. D. Ames, and G. Orosz, "Safety-critical control with input delay in dynamic environment," *IEEE Trans. Control Syst. Technol.*, vol. 31, no. 4, pp. 1507–1520, Jul. 2023.
[38] Y. Chen, G. Orosz, and T. G. Molnar, "Safety-critical connected cruise control: Leveraging connectivity for safe and efficient longitudinal control of automated vehicles," in *Proc. IEEE 27th Int. Conf. Intell. Transp. Syst. (ITSC)*, Sep. 2024, pp. 110–115.
[39] M. Bando, K. Hasebe, K. Nakanishi, and A. Nakayama, "Analysis of optimal velocity model with explicit delay," *Phys. Rev. E, Stat. Phys. Plasmas Fluids Relat. Interdiscip. Top.*, vol. 58, no. 5, pp. 5429–5435, Nov. 1998.
[40] W. Xiao, C. A. Belta, and C. G. Cassandras, "Sufficient conditions for feasibility of optimal control problems using control barrier functions," *Automatica*, vol. 135, Jan. 2022, Art. no. 109960.
[41] Y. Chen, M. Jankovic, M. Santillo, and A. D. Ames, "Backup control barrier functions: Formulation and comparative study," in *Proc. 60th IEEE Conf. Decis. Control (CDC)*, Dec. 2021, pp. 6835–6841.
[42] A. D. Ames, G. Notomista, Y. Wardi, and M. Egerstedt, "Integral control barrier functions for dynamically defined control laws," *IEEE Control Syst. Lett.*, vol. 5, no. 3, pp. 887–892, Jul. 2021.
[43] S. Guo, G. Orosz, and T. G. Molnar, "Connected cruise and traffic control for pairs of connected automated vehicles," *IEEE Trans. Intell. Transp. Syst.*, vol. 24, no. 11, pp. 12648–12658, Nov. 2023.
[44] T. G. Molnár, M. Hopka, D. Upadhyay, M. Van Nieuwstadt, and G. Orosz, "*Virtual rings on highways: Traffic control by connected automated vehicles*," in *AI-enabled Technologies for Autonomous and Connected Vehicles*. Cham, Switzerland: Springer, 2023, pp. 441–479.
[45] M. Nagumo, "Über die Lage der integralkurven gewöhnlicher differentialgleichungen," in *Proc. Physico-Math. Soc.*, vol. 24, 1942, pp. 551–559.
[46] A. D. Ames, X. Xu, J. W. Grizzle, and P. Tabuada, "Control barrier function based quadratic programs for safety critical systems," *IEEE Trans. Autom. Control*, vol. 62, no. 8, pp. 3861–3876, Aug. 2017.
[47] X. Xu, P. Tabuada, J. W. Grizzle, and A. D. Ames, "Robustness of control barrier functions for safety critical control," *IFAC-PapersOnLine*, vol. 48, no. 27, pp. 54–61, 2015.
[48] Q. Nguyen and K. Sreenath, "Exponential control barrier functions for enforcing high relative-degree safety-critical constraints," in *Proc. Amer. Control Conf. (ACC)*, 2016, pp. 322–328.
[49] W. Xiao and C. Belta, "Control barrier functions for systems with high relative degree," in *Proc. IEEE 58th Conf. Decis. Control (CDC)*, Nice, France, Dec. 2019, pp. 474–479.



Yuchen Chen (Graduate Student Member, IEEE) received the B.Sc. degree in mechanical engineering from South China University of Technology, China, in 2022, and the M.Sc. degree from the University of Michigan, Ann Arbor, USA, in 2024, where he is currently pursuing the Ph.D. degree in mechanical engineering. His current research interests include control of connected autonomous vehicles, safety-critical control, and vehicle dynamics.



Gábor Orosz (Senior Member, IEEE) received the M.Sc. degree in engineering physics from Budapest University of Technology and Economics, Hungary, in 2002, and the Ph.D. degree in engineering mathematics from the University of Bristol, U.K., in 2006. From 2017 to 2018, he was a Visiting Professor in control and dynamical systems with California Institute of Technology. In 2022, he was a Distinguished Guest Researcher in applied mechanics with Budapest University of Technology and Economics. From 2023 to 2024, he was a Fulbright Scholar with Budapest University of Technology and Economics. He is currently a Professor of mechanical engineering and a Professor of civil and environmental engineering with the University of Michigan. His research interests include nonlinear dynamics and control, time delay systems, machine learning, and data-driven systems with applications to connected and automated vehicles, traffic flow, and biological networks.



Tamas G. Molnar (Member, IEEE) received the B.Sc. degree in mechatronics engineering and the M.Sc. and Ph.D. degrees in mechanical engineering from the Budapest University of Technology and Economics, Hungary, in 2013, 2015, and 2018, respectively. He has been an Assistant Professor of Mechanical Engineering at the Cleveland State University since 2026. Beforehand, he was an Assistant Professor at the Wichita State University from 2023 to 2026. He held Post-Doctoral Positions at the California Institute of Technology, from 2020 to 2023, and at the University of Michigan, Ann Arbor, from 2018 to 2020. His research interests include nonlinear dynamics and control, safety-critical control, and time delay systems with applications to connected automated vehicles, robotic systems, and autonomous systems.